Přírodovědecká fakulta Univerzity Palackého

v Olomouci

Společná laboratoř optiky

Univerzita Palackého
v Olomouci

Návrh a konstrukce zařízení pro kvantové zpracování informace

Dizertační práce

Vojtěch Trávníček

školitel:

doc. Mgr. Karel Lemr, Ph.D.

Olomouc květen 2021

FACULTY OF SCIENCE, PALACKÝ UNIVERSITY

OLOMOUC

JOINT LABORATORY OF OPTICS

Palacký University
Olomouc

Design and construction of devices for quantum information processing

Ph.D. THESIS

Vojtěch Trávníček

supervisor:

doc. Mgr. Karel Lemr, Ph.D.

OLOMOUC MAY 2021

Bibliographic details

Title	Design and construction of devices for quantum information processing
Název	Návrh a konstrukce zařízení pro kvantové zpracování informace
Type	Ph.D. thesis
Author	Vojtěch Trávníček
Supervisor	doc. Mgr. Karel Lemr, Ph.D.
Univesity	Palacký University Olomouc
Study program	P1703 Physics
Department	Joint Laboratory of Optics
Language	English
Year	2021
Pages	86

Declaration of originality

I hereby declare that this thesis is my own work and that, to the best of my knowledge and belief, it contains no material previously published or written by another person nor material which to a substantial extent has been accepted for the award of any other degree or diploma of the university or other institute of higher learning, except where due acknowledgement has been made in the text.

In Olomouc, ...

Submitted on .....

The author grants permission to Palacký University in Olomouc to store and display this thesis and its electronic version in university library and on official website.

Acknowledgment

I would like to express my sincere gratitude to all my colleagues especially to my supervisor Karel Lemr, Ph.D., for irreplaceable leadership and guidance and to Antonín Černoch, Ph.D., Karol Bartkiewicz, Ph.D., Jan Soubusta, Ph.D., Ievgen Arkhipov, Ph.D., and Mgr. Kateřina Jiráková for expert advice, fruitful discussions and much appreciated help in the laboratory.

The author acknowledges the financial support by the Czech Science Foundation under projects No. 19-19002S, No. 20-17765S and also internal Palacky University Grant No. IGA-PrF-2021-004.

The author

Contents

Chapter 1

Introduction

1.1 Quantum optics

Quantum optics is a field of research that focuses on the application of quantum mechanics to the phenomena involving light and its interaction with matter. The term quantum optics was not customary in the first part of 20th century as the research in quantum mechanics was more focused on the properties of matter rather then light. This changed with the developments in laser science in which quantum mechanics underlying the laser's principles was studied with the emphasis on the properties of light [1].

From 1950s the interest in quantum optics rose rapidly as J. Klauder, G. Sudarshan, R. J. Glauber[1] and L. Mandel presented a quantum description of electromagnetic field which provided better understanding of photodetection and photon statistics [2, 3]. This led to an introduction of the coherent state which approximately describes the output of a single-frequency laser and exhibits Poissonian photon number statistics unlike the thermal light where the number of detected photons exhibits Bose-Einstein distribution. Other exotic quantum states, such as squeezed states of light [4] were subsequently discovered. Since development of the laser many areas of research in the topic of quantum optics emerged. Development of short and ultrashort pulses achieved by Q-switching [5] and mode-locking [6] techniques made the research of ultrashort processes possible [7].[2] The study of mechanical forces of light on matter led to levitating and positioning cloud of atoms by optical trap and optical tweezers [8]. A very interesting application of quantum optics and laser science is Doppler [9] and Sisyphus cooling [10] which was crucial for achieving the Bose-Einstein condensation.[3] Experimen-

[1] In 2005 R. J. Glauber received the Nobel price for his contribution to the quantum theory of optical coherence.

[2] In 2018 G. Morou and D. Strickland received the Nobel price for their method of generating high-intensity, ultra-short optical pulses. This price was shared with A. Ashkin for his research in the optical tweezers and their application to biological systems.

[3] In 1997 S. Chu, C. Cohen-Tannoudji and W. D. Phillips were awarded the Nobel Prize for their work in laser cooling and atom trapping.

tal demonstration of quantum entanglement [11, 12], quantum teleportation [13, 14] and the construction of quantum logical gates [15] achieved generally on the optical platform opened the way to the study of quantum information processing and quantum communications. This progress led for example to the possibility for quantum algorithms [16, 17] and information-theoretic secure communications [18–20].

The study of quantum physics and using the quantum laws of nature for our benefit already did bring us better understanding of the workings of our universe and innovations which would be hard to give up. Nevertheless there are still many questions unanswered and the possibility for improvement of our technology is almost limitless.

1.2 Quantum information processing

Quantum information processing (QIP) is diverse and interdisciplinary field of research including quantum information theory, quantum communications, quantum computation, quantum algorithms and their complexity and quantum control. It relies on the use of laws of quantum physics to improve the above mentioned areas of quantum information science with respect to their classical counterparts [21].

The basis for these improvements is the information encoding. While current classical computers encode information into bits which are binary, quantum computers encode information into qubits [22] which can exist in superposition. This and other phenomena of quantum physics[4] potentially enable quantum computers to solve certain problems much faster then any classical computer.

For instance, a well known example of a quantum algorithm that, in principle, runs faster then it would be possible with known classical approach is the Shor's algorithm [17]. It is theoretically capable to factorize the product of large prime numbers in polynomial time, almost an exponential speed-up compared to known classical factoring algorithms. There have been several experimental demonstrations of the Shor's algorithm [23, 24], although these were able to factorize only double-digit numbers.[5]

Nevertheless, the potential efficiency of quantum algorithms is so significant that they pose a threat to commonly used classical cryptographic methods. It is again quantum mechanics that provides possible solution to these security concerns. The so-called quantum cryptography [19, 20] makes use of quantum mechanical properties of quantum states such as the impossibility of perfect cloning [18] to provide information-theoretic secure distribution of information.

[4] such as quantum entanglement

[5] In 2012 two groups demonstrated the factorization of numbers 15 and 21.

However, no-cloning theorem also makes the distribution of quantum information (qubits) over long distances not an easy task. It is due to signal degradation within the quantum channel [25]. Therefore, a quantum approach to overcome transmission loss is required. Solution can be provided by the quantum entanglement, a phenomenon achievable between at least two qubits. Devices based on the entanglement swapping protocol [26] such as quantum relay or repeater in principle split the transmission distance into smaller segments lowering the error probability [25, 27]. There are many challenges involved in the development of quantum relays or repeaters as they are complex systems requiring sophisticated quantum devices and routines such as quantum memories [28, 29] and entanglement distillation [30, 31].

QIP schemes can be realized on several physical platforms including trapped ions, nuclear magnetic resonance, cavity quantum electrodynamics and linear optics [32–34, A1]. The platforms where information is stored in the properties of electrons or ions is better suited for quantum computing, complex logical gates or quantum memory. The linear optics platform on which qubits are encoded into properties of light (photons) seems particularly suitable for quantum communications as photons are fast, well controllable and mostly unaffected by environment [35–38]. As this area of research is very promising many quantum communications protocols and QIP schemes, including those presented in this theses, are being proposed and experimentally implemented.

1.3 Quantum machine learning

Machine learning is study of data analysis techniques that use computational methods to learn (seek patterns in empirical data) without relying on a predetermined explicitly formulated model. The learning algorithms are based on minimizing a constrained multivariate function, where the result of this optimization is a decision function that maps input points to output points. In other words, machine learning algorithms build a mathematical model based on training data in order to make predictions or decisions without being explicitly programmed to do so. Machine learning has become a key technique for solving complex tasks involving large amount of data and lots of variables. Such as email filtering, face and speech recognition, self-driving cars and algorithmic trading [39].

The term quantum machine learning most often refers to machine learning algorithms for the analysis of classical data, where the whole task or just computationally difficult subroutines are outsourced to quantum device, i.e. quantum-enhanced machine learning [40–42]. Computational complexity of an algorithm is defined as the amount of resources (time, memory, number of arithmetic operations) required to solve a problem. In computer science, the computational complexity is standardly described in terms of the Big $\mathcal{O}$ notation [43]. It is used

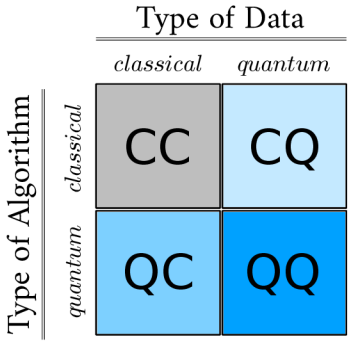

Figure 1.1: Four different approaches to combine the disciplines of quantum computing and machine learning.

to classify algorithms according to the growth of requirements with respect to the growth of the inputs.[6] It has been already demonstrated that by quantum approach one can reduce the complexity of several algorithms used as subroutines in machine learning [44–47]. One can also consider convexity which is often desired in machine learning. Convex optimization problems are not sensitive to initial conditions and do not fail due to local extrema. Finding the minimum of a loss function is then relatively fast, simple and less computationally intensive. However, many optimization problems such as neural networks are generally non-convex [48]. Even though some of these problems are differentiable, meaning that they can be decomposed to a number of convex problems, there are some non-convex optimization algorithms, such as evolutionary algorithms, which show several advantages for learning. For instance, sparser models ensure better generalization performance, and non-convex objective functions are less sensitive to noise and outliers [49]. For this reason, non-convex optimization algorithms seem to be gaining more and more recognition in the machine learning community. This approach to optimization might prove easier and faster to solve by quantum computing as quantum algorithms look for the optimum through different, more physical, process and are not bound by convexity restrictions [40].

1.4 Outline

The main part of this thesis consists of three genuine QIP experiments realized on the linear optical platform. These experiments were performed at the Joint Laboratory of Optics of Palacký University and Czech Academy of Sciences. The Quantum Optics group at this institution has a lot of experience and rich history of research in quantum information processing [50–52].

[6] For example, notation $\mathcal{O}(x^2)$ states that requirements of a certain algorithm grow quadratically as $x \to \infty$.

1.4.1 Experiment 1: Measurement of a non-linear entanglement witness by hyper-entangling two-qubit states

Based on *Vojtěch Trávníček, Karol Bartkiewicz, Antonín Černoch, and Karel Lemr Phys. Rev. A* ***98****, 032307 (2018).*

The first experiment presented in this thesis discusses the problem of entanglement detection. Quantum entanglement is one of the key phenomenon in quantum physics [53, 54]. It plays a crucial role in quantum communications and quantum computing, therefore, it is the subject of intense investigation [15, 55]. In the experiment we demonstrate that non-linear entanglement witnesses can be made particularly useful for entanglement detection in hyper-entangled or multilevel states.

For the purposes of demonstrating this concept, one of the less complex non-linear entanglement witnesses known as the collectibility was selected. The original technique which was proposed by Rudnicki *et al.* [56, 57] allows to detect entanglement in large number of two-qubit states. The collectibility measurement of systems entangled in one degree of freedom requires to perform the collective measurements on two identical copies of the investigated state. This was later experimentally realized by Lemr *et al.* [58]. The presented experiment shows that collectibility can be measured directly on a single multilevel state where a two-qubit state is copied across two degrees of freedom. This approach was tested for three characteristic two-qubit quantum states. The experiment was performed in 2017 and published year later.

1.4.2 Experiment 2: Measurement of the Hilbert-Schmidt distance between two-qubit states

Based on *Vojtěch Trávníček, Karol Bartkiewicz, Antonín Černoch, and Karel Lemr Phys. Rev. Lett.* ***123****, 260501 (2019).*

The second experiment addresses distance measurements in Hilbert space. The measurement of distance between quantum states is an important tool for the field of quantum communications, where the transmission channel accuracy can be determined by measuring distances between transmitted and received states. These distance measures are also essential for certain classification algorithms as the common method is to perform distance measurements among sample vectors [40]. The most prominent distance measures include Uhlmann-Jozsa fidelity (Bures metrics), trace distance and Hilbert-Schmidt distance [59, 60, A2].

The experiment aims to demonstrate the measurement of Hilbert-Schmidt distance between characteristic two-qubit states. It shows that the new method for measuring distances in Hilbert space is far less complex than reconstructing den-

sity matrices and that it can be applied in quantum-enhanced machine learning to reduce the complexity of calculating Euclidean distances between multidimensional points. The results are also a novel example of applying mixed states in quantum information processing. Usually working with mixed states is undesired, but here it gives the possibility of encoding extra information in the coherence between given two dimensions of the density matrix. The experiment was performed in 2019 and published in the same year.

1.4.3 Experiment 3: Diagnostics of entanglement swapping by a collective entanglement test

Based on *Vojtěch Trávníček, Karol Bartkiewicz, Antonín Černoch, and Karel Lemr, Phys. Rev. Applied,* ***14****, 064071 (2020).*

The third experiment discusses the diagnostics of entanglement swapping protocol [26] by means of collective entanglement witness [56, 57]. Since entanglement swapping is a key procedure for quantum repeaters [25], quantum relays [27], device-independent quantum communications or entanglement assisted error correction [61, 62], this can aid in faster and practical resolution of quality-of-transmission related problems as this approach requires fewer measurements then other means of diagnostics.

In this experiment we make use of similarities shared between a non-linear entanglement witness and an entanglement swapping device. By measuring individual quantities used to calculate this non-linear witness, we simultaneously obtain useful data that allow to identify any imperfections in the entanglement swapping.

The experiment demonstrates that this approach is suitable to detect disturbances occurring in the preparation of quantum states, quantum communication channel and imperfect Bell-state projection. The experiment was performed in 2019 and published in 2020.

Chapter 2

Methods and tools

2.1 Hilbert space

A state of a physical system is in quantum mechanics represented by a vector in Hilbert space ($\mathcal{H}$) [63]. The term Hilbert space often refers to an infinite-dimensional complex vector space with inner product that is complete or closed. However, in quantum information processing it is also used in context of finite-dimensional spaces, where the condition of completeness is automatically satisfied.[1] The vectors in $\mathcal{H}$ are in quantum mechanics usually denoted using Dirac notation as $|v\rangle$ called a *ket*, where v is the "name" of the vector. The inner product is then defined as $\langle u|v\rangle$, where $\langle u|$ is called a *bra* which is a hermitian conjugate (conjugate transpose) to $|u\rangle$. A collection of linearly independent vectors $\{|v_i\rangle\}$ forms a basis of $\mathcal{H}$ if every element of $\mathcal{H}$ ($|\psi\rangle$) can be written as linear combination of these vectors as

$$|\psi\rangle = \sum_{i}^{d} c_i |v_i\rangle, \tag{2.1}$$

where d is dimension of $\mathcal{H}$. Particularly useful are basis vectors that are orthogonal and complete with following properties

$$\langle v_i|v_j\rangle = \delta_{ij}, \tag{2.2}$$

$$\sum_{i}^{d} |v_i\rangle\langle v_i| = 1, \tag{2.3}$$

[1] This is true when one encodes information into individual physical objects such as photons.

where δ_{ij} is the Kronecker delta. It is often convenient to think of kets and bras as column and row vectors respectively

$$|\psi\rangle = \begin{bmatrix} c_1 \\ c_2 \\ \vdots \\ c_d \end{bmatrix} \qquad \langle\psi| = \begin{bmatrix} c_1^\star, & c_2^\star, & \ldots, & c_d^\star \end{bmatrix}. \tag{2.4}$$

Note that the numbers c_i and $c_i^\star$ depend on the choice of basis, while the inner product is independent.

2.1.1 Kets and physical properties

Two vectors $|\psi\rangle$ and $\xi|\psi\rangle$, where $\xi|\psi\rangle$ is a scalar multiplication of $|\psi\rangle$ by a non-zero complex number ξ, have in quantum mechanics the same physical significance. For this reason, one might say that the state of a physical system is not represented by a vector, but rather by a ray defined as a collection of all the complex multiplications of the given vector.

The complex number ξ can always be chosen so that the quantum state $|\psi\rangle$ representing the physical system is normalized

$$\langle\psi|\psi\rangle = 1. \tag{2.5}$$

Working with normalized vectors is often convenient as in quantum mechanics one usually looks for probabilities of finding a physical system described by $|\psi\rangle$ in some quantum state e.g., $|\phi\rangle$. This probability is defined by the inner product of these two vectors as

$$|\langle\phi|\psi\rangle|^2, \tag{2.6}$$

where the normalization condition ensures that the inner product has dimension of probability. Note that one can multiply normalized vector by a phase $e^{i\varphi}$, where φ is real without changing the normalization or physical meaning. Thus normalization does not produce a unique vector representation of a given physical system.

Keep in mind that just because $|\psi\rangle$ and $\xi|\psi\rangle$ have the same physical significance does not mean that one can multiply a vector inside a linear combination by a constant without changing the physical interpretation. Note that $|\phi\rangle + |\psi\rangle$ and $|\phi\rangle - |\psi\rangle$ do not, in general, represent the same physical system.

2.2 Qubit

In classical information theory the basic unit of information is called a bit (binary digit). As the name suggests the bit represents a logical state with one of two

possible values usually represented by numbers "0" and "1". Physically, the bits are most commonly encoded into electrical voltage, current or light intensity. The most important fact about the bit from the quantum physics point of view is that it theoretically possesses the logical value "0" or "1" with absolute certainty [64].

This is not the case with the qubit, which is a unit of quantum information [22]. It is due to one of the fundamental principle of quantum physics, which is the quantum superposition. The principle states that if a physical system may be in one of multiple configurations then the most general pure state of the system is a linear combination of all these possibilities. For instance, for a pure quantum state of a qubit with two orthonormal basis states $|0\rangle$ and $|1\rangle$ the most general state would be

$$|\Psi\rangle = \alpha|0\rangle + \beta|1\rangle.$$

The coefficients α, β are generally complex numbers associated with probability amplitudes, therefore, they obey the normalization constrained

$$|\alpha|^2 + |\beta|^2 = 1.$$

Qubit is then formally defined as normalized vector in a two-dimensional Hilbert space. Note that the state of the qubit in superposition is not somewhere in between the basis states, rather, when measured, the qubit is with probability $|\alpha|^2$ ($|\beta|^2$) found in state $|0\rangle$ ($|1\rangle$) [21].

In order to physically encode a qubit, one requires an object that supports a two-level quantum system. This object might be an electron, ion, Josephson junction or a photon. A qubit can be encoded into the state of photons in multiple ways, however, there are two distinct approaches. Firstly, it is individual photon encoding such as polarization (e.g., [14, 65]), spatial mode (e.g., [50, 66]) and time-bin encoding (e.g., [67]). These are also known as discrete variables. The second approach uses collective multiphoton states and is often related to the so-called continuous variables for example light quadratures [68, 69]. Note that in hereby presented experiments qubits were encoded into the discrete variables namely into polarization and spatial modes.

Encoding into polarization degree of freedom is widely used especially in QIP realized in bulk optics. The mapping of qubit state onto polarization state of a photon is quite straightforward as they both occupy the same two-dimensional Hilbert space. It is useful to visualize polarization state of a photon using the Bloch sphere, where horizontal and vertical polarizations sit on the poles, meanwhile their balanced superpositions are situated on the equator (see Figure 2.1). It is customary to associate horizontal and vertical polarizations with logical qubit states $|0\rangle$ and $|1\rangle$ respectively. Due to equivalent representations of states via the Bloch diagram, any state on the surface of the Bloch sphere can be written as $|\Psi\rangle = \cos\frac{\theta}{2}|H\rangle + \mathrm{e}^{i\varphi}\sin\frac{\theta}{2}|V\rangle$.

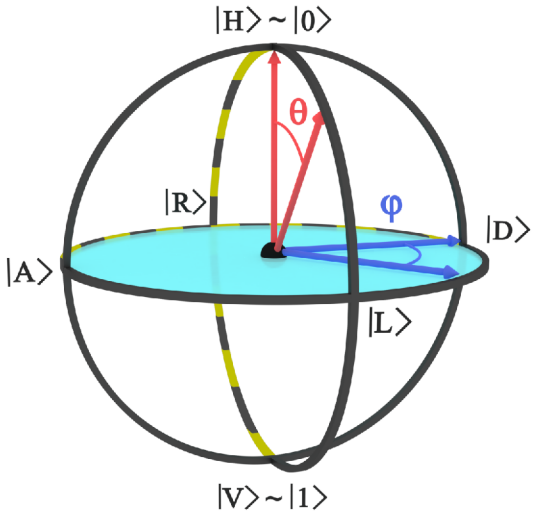

Figure 2.1: Visualization of the Bloch sphere. Horizontal polarization state $|H\rangle$ represents logical qubit state $|0\rangle$ while vertical polarization state $|V\rangle$ corresponds to logical qubit state $|1\rangle$. The depiction also includes positions of balanced superposition states situated on the equator. Diagonal and anti-diagonal linear polarization states are labeled $|D\rangle$ and $|A\rangle$. Right-hand and left-hand circular polarization states are denoted $|R\rangle$ and $|L\rangle$ (see Table 2.1).

Another degree of freedom that can be employed to encode quantum information are the spatial modes of a photon. Here, the presence of a photon on a certain path is designated logical state $|0\rangle$ or $|1\rangle$ (see Figure 2.2). Note that using a general fiber coupler one can also prepare a superposition of the two modes. Spatial mode encoding is predominantly used in fiber-optical setups as polarization state of a photon is prone to change during propagation in a standard optical fiber.

Viable option is also to encode multiple qubits into multiple degrees of freedom of a single photon [A1, A3]. This approach allows one to encode more information into the available number of photons, however, it makes building the desired QIP scheme more challenging. An example of this mixed encoding is presented in the first two experiments included in this thesis. In both cases polarization and spatial degree of freedom were used to encode two qubits of information into a single photon.

2.3 Photons for quantum information processing

Quantum information processing schemes realized with individual discrete photons and linear optics rely on photon interference for the desired photonic interactions to take place. This means that the photons should be close to ideal Fock $|1\rangle$ states and highly indistinguishable in their wavelength, polarization, spatial mode

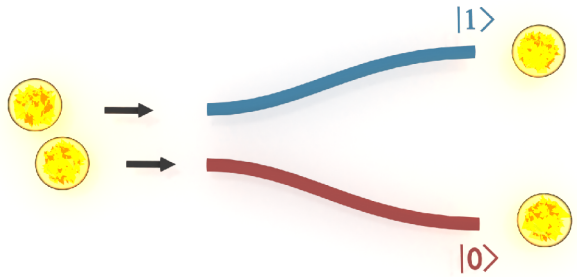

Figure 2.2: Schematic depiction of spatial encoding. Photon in the upper path represents logical qubit state $|1\rangle$ while photon in the lower path logical qubit state $|0\rangle$.

and time of arrival. Therefore, it is evident that preparation of suitable photons is a necessary condition for experimental implementation of the QIP schemes. This sections provides a brief description of the principle of the photon source employed in the later presented experiments.

The source is based on a non-linear process commonly known as spontaneous parametric down conversion (SPDC) observable under certain conditions in a medium with a $\chi^{(2)}$ optical non-linearity pumped by strong optical field [70, 71]. The interaction between the pump beam and the medium might result in decay of a pump photon (p) into a pair of time correlated photons called signal (s) and idler (i) of lower energy. The spectral properties and spatial geometry of the generated photons are determined by the conservation laws of energy and momentum (phase-matching condition)

$$\hbar\omega_\mathrm{p} = \hbar\omega_\mathrm{s} + \hbar\omega_\mathrm{i}, \qquad \hbar\vec{k}_\mathrm{p} = \hbar\vec{k}_\mathrm{s} + \hbar\vec{k}_\mathrm{i}, \tag{2.7}$$

together with the configuration and characteristics of the medium. The phase-matching condition has dramatic effect on the efficiency of the SPDC process and therefore, should be maintained for the entire length of the medium. However, it is very difficult to fulfill the phase-matching condition in homogeneous isotropic materials. It is due to chromatic dispersion where the interacting waves experience different index of refraction which causes phase mismatch

$$|\Delta\vec{k}| = |\vec{k}_\mathrm{p}| - |\vec{k}_\mathrm{s}| - |\vec{k}_\mathrm{i}| \neq 0. \tag{2.8}$$

One way how to mitigate the phase mismatch is to use birefringent materials, typically $LiIO_3$ or β-BaB_2O_4 (BBO), where the refractive index not only depends on frequency, but also on the polarization and direction of the light propagating through the crystal. The phase matching condition is then fulfilled by suitable polarization of the waves and orientation of the crystal. There are several types

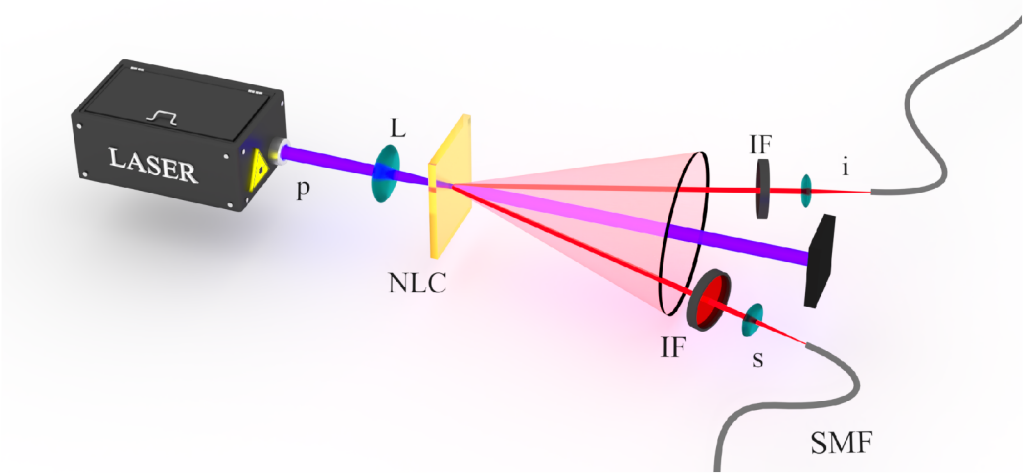

Figure 2.3: Simplified scheme of a source of photon pairs based on the SPDC process: The pumping beam is focused by a lens (L) and impinges on the non-linear crystal (NLC), where a pumping photon (p) might decay into a pair of time correlated photons called signal (s) and idler (i). These photons are then collected by couplers into single-mode optical fibers (SMF). In order to ensure the wavelength indinstinguishability of the generated photons and to prevent the diffracted pumping photons from entering the fibers, cut-off or interference filters (IF) are positioned in front of the couplers.

of birefringent phase matching that differ in polarization states of the input and output photons. In the presented experiments only the non-collinear type I phase matching was used, where extraordinary polarized pumping photon generates two photons with ordinary polarization that leave the crystal on opposite sides of a cone centered around the pumping beam (see Figure 2.3). As it was mentioned earlier, the photons must be highly indistinguishable this requires precise positioning of photon couplers, single-mode optical fibers and spectral filtering by cut-off or interference filters.

Note that the source generates time correlated photon pairs whose polarization state can be in an ideal case described by a pure separable state, for instance $|HH\rangle$. Although separable states are suitable for many QIP schemes, there are QIP protocols, such as quantum teleportation or quantum repeater, that rely on entangled photon states.

2.3.1 Generation of entangled photon pairs

One non-linear crystal with type I phase matching can not directly produce polarization entangled photon pairs. Indirect polarization entanglement is achievable afterwards by means of post-selection [72]. This approach however, requires the post-selection to be compatible with the rest of the QIP scheme which is not always feasible. One can generate polarization entangled photons directly by means

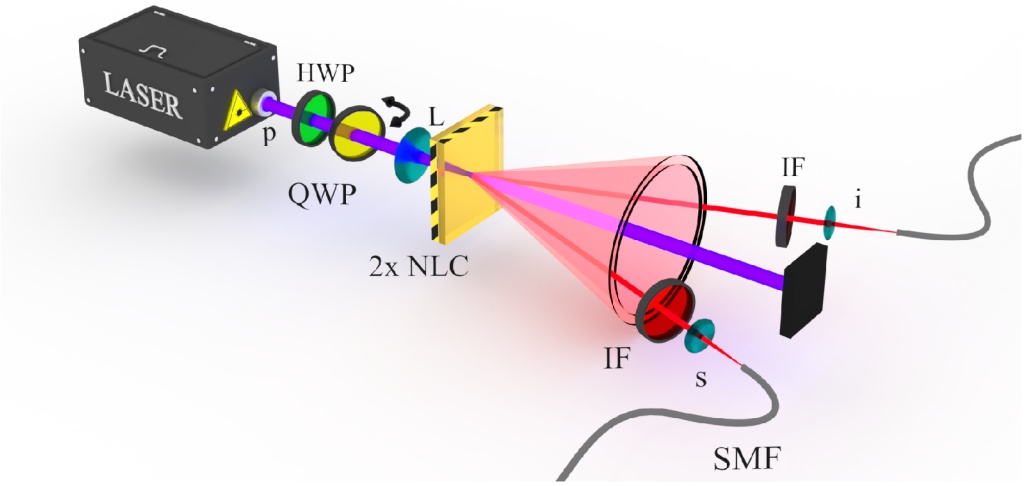

Figure 2.4: Simplified scheme of a source of polarization entangled photon pairs based on the Kwiat source: The pumping beam is focused by a lens (L) and impinges on two non-linear crystals (NLC) mutually rotated by 90°. The directions of the optical axes of the crystals are represented by red and black stripes. Due to indistinguishable point of origin of the photon pair and generally elliptical polarization of the pumping beam the polarization state of the two photons is in the form Eq. (2.9). The photons then pass through cut-off or interference filters (IF) to ensure the wavelength indinstinguishability and are collected by couplers into single-mode optical fibers (SMF). The polarization state of the pumping beam is tuned by half-wave plate (HWP) and quarter-wave (QWP) plate in front of the crystals.

of type II phase matching [14]. During this process extraordinary polarized pumping photon decays into two photons with orthogonal polarizations. The generated photons leave the crystal in a direction of two cones (one for each polarization) which are symmetrical to the pumping beam. The amount of overlap between the cones depends on the orientation of the crystal (orientation of it's optical axis) and the angle of incidence of the pumping beam. Polarization entangled photon pairs then can be observed at the cross-section of the two cones. Due to the orthogonal polarizations of the signal and idler photons there are effects known as walk-off that reduce the quality of the entanglement. The polarization dependent refractive indices cause the separation of the signal and idler beams called transversal walk-off meanwhile different group velocities cause longitudinal walk-off. This negative effects can be mitigated by compensation optics [70].

A photon source that produces polarization entangled photon pairs and does not have problems with walk-off was realized by Kwiat *et al.* [73]. The source, depicted in Figure 2.4, consists of two non-linear crystals cut for type I phase matching mutually rotated by 90°. Hence, the down-converted photons created in one crystal have orthogonal polarization with respect to the photons created in

the other crystal. Note that if the pumping beam is polarized so that both horizontal and vertical polarization components are non-zero either of the crystals is capable of down-conversion. In order to prepare an entangled state, the couplers must collect photon pairs from both crystals simultaneously. This is achieved by combination of several aspects such as the thickness of the crystals[2] and the angle between propagation direction of the pumping beam and generated photons.[3] Thinner crystals and tighter angles improve spatial overlap of the photons generated from both crystals. However, they also lower the probability of down-conversion event and make the manipulation with the couplers more difficult as the couplers are now closer to the pumping beam. The later can be mitigated by increasing the distance between the crystals and the couplers.[4] Combining these aspects ensures that paths of the generated photons from both crystals are almost identical, therefore, the couplers can not distinguish in which crystal the photon pair originated. This makes the polarization state of the photon pair a coherent superposition of separable states $|HH\rangle$ and $|VV\rangle$.

The Kwiat source generally produces polarization entangled two-photon states in the form of

$$|\psi\rangle = \cos(\alpha)|HH\rangle + \mathrm{e}^{i\theta}\sin(\alpha)|VV\rangle, \tag{2.9}$$

where the parameters α, θ are connected to the polarization state of the pumping beam. The ratio between the $|HH\rangle$ and $|VV\rangle$ components is affected by parameter α which can be modified by rotating a half-wave plate in the pumping beam. Parameter θ affects the phase between the components. The phase can be changed by tilting a quarter-wave plate in front of the crystals. Note that for $\alpha = \pi/2$ both crystals are pumped equally and the source generates maximally entangled states.

2.4 Linear optical toolbox

Manipulation with the photons and thus processing the information stored in their states is achieved by a series of linear optical tools [1, 74]. This section describes several of these optical elements employed in the presented experiments.

2.4.1 Beam splitter

One of the most important tools for QIP realized on the platform of linear optics is presumably the beam splitter. Physically, it usually takes the form of a semi-transparent mirror which transmits only a certain portion of the incident light

[2] in our case 0.6 mm

[3] In the presented experiments the angle between the pumping beam and the photons was about 4°.

[4] in our case 1 m

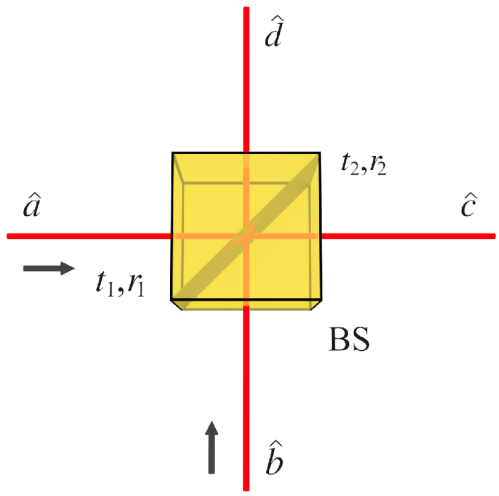

Figure 2.5: Conceptual scheme of a cube beam splitter: Optical fields in the input ports characterized by annihilation operators $\hat{a}$ and $\hat{b}$ are being coherently mixed according to the beam splitter transformation described in Eq. (2.11)

while reflecting the rest. There are several beam splitter constructions, for instance, cube and plate beam splitters for bulk optics or fiber beam splitter (FBS) for fiber optics. In classical description, beam splitter transforms incident light with amplitude E into the transmitted and reflected beams which amplitudes are given by

$$E_t = t_1 E, \qquad E_r = r_1 E, \tag{2.10}$$

where t_1 and r_1 are the transmission and reflection amplitudes respectively. In quantum theory the amplitudes of the field are replaced by Heisenberg annihilation operators $E \to \hat{a}, E_t \to \hat{c}, E_r \to \hat{d}$ [2]. To make sure that these annihilation operators fulfill commutation relations, one needs to consider both input ports of the beam splitter even if one of the ports is in vacuum state (Fock state $|0\rangle$). Thus in quantum mechanical description the beam splitter is characterized by transmission t_i and reflection r_i amplitudes in two input ports (see Figure 2.5). A phase shift between the transmission and reflection introduced at the interface is usually associated only with one of the beams. Let transmission coefficient t_i be a real number, thus the information about the relative phase shift is carried by the reflection coefficient $r_i e^{i\varphi_i}$. Then the action of lossless beam splitter can be described in matrix formalism by

$$\begin{pmatrix} \hat{c} \\ \hat{d} \end{pmatrix} = \begin{pmatrix} t_1 & r_2 e^{i\varphi_2} \\ r_1 e^{i\varphi_1} & t_2 \end{pmatrix} \begin{pmatrix} \hat{a} \\ \hat{b} \end{pmatrix} = U \begin{pmatrix} \hat{a} \\ \hat{b} \end{pmatrix}, \tag{2.11}$$

where the transformation matrix U has to be unitary in order to ensure the validity of commutation relations for the Heisenberg operators. Assuming $|t_1| = |t_2|, |r_1| = |r_2|$ leads to

$$U^\dagger U = \begin{pmatrix} t^2 + r^2 & tr(e^{i\varphi_2} + e^{-i\varphi_1}) \\ tr(e^{i\varphi_1} + e^{-i\varphi_2}) & t^2 + r^2 \end{pmatrix} = \begin{pmatrix} 1 & 0 \\ 0 & 1 \end{pmatrix}. \tag{2.12}$$

It is evident that for a lossless beam splitter $t^2 + r^2 = 1$. Also from

$$e^{i\varphi_1} + e^{-i\varphi_2} \equiv 2e^{i(\varphi_1 - \varphi_2)/2} \cos\frac{\varphi_1 + \varphi_2}{2} = 0, \tag{2.13}$$

one concludes that $\varphi_1 + \varphi_2 = \pi$ where the consensus is to set $\varphi_1 = \frac{\pi}{2}$ and $\varphi_2 = \frac{\pi}{2}$ (Beam splitter with symmetrical phase shift). Then the transformation matrix takes the form of

$$U = \begin{pmatrix} t & ir \\ ir & t \end{pmatrix}. \tag{2.14}$$

It is the linear relation Eq. (2.11) for the operators that makes the linear optics called "linear".

2.4.2 Polarization sensitive beam splitter

QIP schemes based on the popular polarization encoding require optical components that are sensitive to the polarization state of the incident photons. It is needed for controlling the polarization degree of freedom of individual photons in order to process the quantum information. One of these components is a polarization sensitive beam splitter (PSBS) which exhibits different reflection coefficients for horizontal and vertical polarization components of the incident light. This complicates the mathematical description of an ideal PSBS as both polarization components require separate input and output modes (see Figure 2.6)

$$\begin{pmatrix} \hat{c}_\mathrm{h} \\ \hat{c}_\mathrm{v} \\ \hat{d}_\mathrm{h} \\ \hat{d}_\mathrm{v} \end{pmatrix} = \begin{pmatrix} t_\mathrm{h} & 0 & ir_\mathrm{h} & 0 \\ 0 & t_\mathrm{v} & 0 & ir_\mathrm{v} \\ ir_\mathrm{h} & 0 & t_\mathrm{h} & 0 \\ 0 & ir_\mathrm{v} & 0 & t_\mathrm{v} \end{pmatrix} \begin{pmatrix} \hat{a}_\mathrm{h} \\ \hat{a}_\mathrm{v} \\ \hat{b}_\mathrm{h} \\ \hat{b}_\mathrm{v} \end{pmatrix}, \tag{2.15}$$

where indices h and v denote horizontal and vertical polarization in relation to the plane of incidence. In the experiments presented in later chapters cube PSBSs were used. The cube is often made of two triangular glass prisms that are attached by a transparent resin or cement. The polarization sensitive beam splitters were used as polarizators (PBS) for which the typical values of transmission and reflection coefficients are $|t_\mathrm{h}|^2 > 90\%$ and $|r_\mathrm{v}|^2 > 99.5\%$. The action of PBS then separates the two polarization components by reflecting one of them with dielectric coating which is applied to the hypotenuse of one of the prisms. Con-

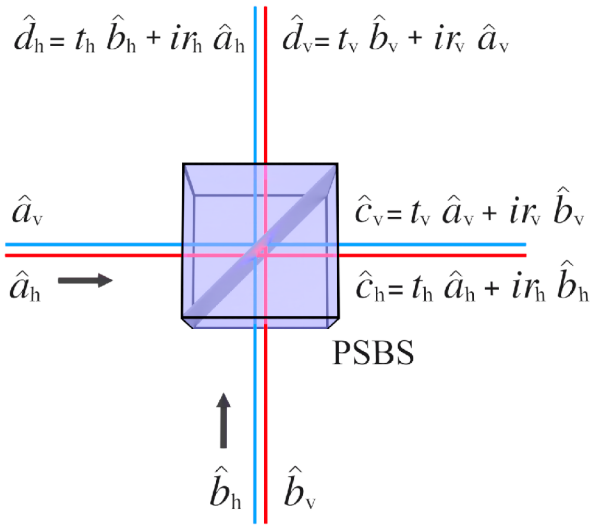

Figure 2.6: Conceptual scheme of a polarization sensitive beam splitter cube: Generally, the orthogonal polarization components do not experience the same splitting ratio. This is due to polarization sensitive reflection coating which introduces different reflection coefficients for the two polarization components of the incident light. Note that in a spatial case PSBS can act as polarizing beam splitter.

struction of the cube PBS ensures a 90° separation between the horizontal and vertical polarization and a minimal transverse offset of the transmitted beam. Note that the action of PBS can be used for spatial encoding which is described in the previous Section 2.2.

2.4.3 Beam displacer

Beam displacer (BD) is similar to a PBS in separating incident light into two orthogonally polarized beams, however, there are few important differences. Unlike PBS, the beam displacer used in the conducted experiments was manufactured from birefringent material such as calcite. Due to it's birefringent nature, light polarized perpendicular to a plane defined by the optical axis and direction of propagation experiences a different index of refraction than light which is polarized parallel to the plane. Moreover due to the fact that the optical axis is not parallel or perpendicular to the incident spatial mode, a walk-off effect is observed for one polarization. Therefore, the incident light is laterally separated into two orthogonally polarized beams that exit the crystal by the same side. For reference see Figure 2.7. The displacement (d) of the two polarization states can be calculated as

$$d = L\tan(\alpha), \tag{2.16}$$

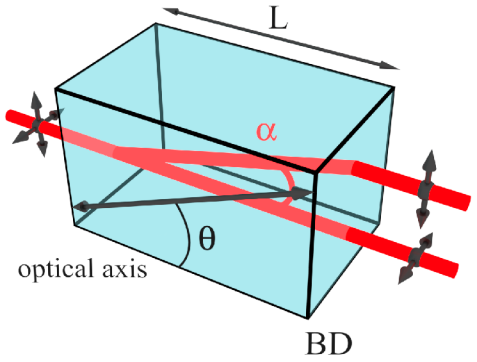

Figure 2.7: Conceptual scheme of a beam displacer: The beam displacer separates horizontal and vertical polarization components of the incident light by birefringence and orientation of an optical axis. Note that optical field in the displaced path is polarized parallel to the plane defined by the optical axis and direction of propagation while optical field in the unchanged path is polarized perpendicularly.

$$\tan(\alpha) = \left(1 - \frac{n_\mathrm{o}^2}{n_\mathrm{e}^2}\right) \frac{\tan(\theta)}{1 + \frac{n_o^2}{n_e^2}\tan^2(\theta)}, \tag{2.17}$$

where n_o and n_e are the ordinary and extraordinary refraction indices respectively. Typical distance between the outgoing beams is for commercially available calcite beam displacers in a range of few millimeters. Depending on the construction and material of the BD the outgoing beams might be parallel or divergent.

2.4.4 Wave plates

Another polarization controlling devices are birefringent wave plates, or retardation plates. These optical elements transmit light and modify its polarization state without attenuating, deviating, or displacing the beam.[5] They are extremely useful when one needs to manipulate the polarization of light within a single spatial mode. A wave plate is a thin wafer of a uniaxial crystal, typically quartz, which is cut in a way that the plane of the wafer contains the fast and slow optical axis. In this case the optical axis is perpendicular to the designated incident spatial mode. Light polarized along fast axis encounters lower index of refraction and travels faster through wave plate than light polarized along the slow axis. Thus, the wave plate introduces a relative phase Γ between those two components, which is related to the birefringence $\Delta n = n_\mathrm{e} - n_\mathrm{o}$ and the thickness L of the crystal by the formula

$$\Gamma = \frac{2\pi\Delta n L}{\lambda_0}, \tag{2.18}$$

[5]This is a case for zero angle of incidence.

Table 2.1: Jones vectors and matrices for polarized light and wave plates.

Polarization	ket notation	Jones vector
horizontal	$\|H\rangle$	$\begin{pmatrix}1\\0\end{pmatrix}$
vertical	$\|V\rangle$	$\begin{pmatrix}0\\1\end{pmatrix}$
diagonal	$\|D\rangle = \frac{1}{\sqrt{2}}(\|H\rangle + \|V\rangle)$	$\frac{1}{\sqrt{2}}\begin{pmatrix}1\\1\end{pmatrix}$
anti-diagonal	$\|A\rangle = \frac{1}{\sqrt{2}}(\|H\rangle - \|V\rangle)$	$\frac{1}{\sqrt{2}}\begin{pmatrix}1\\-1\end{pmatrix}$
right-hand circular	$\|R\rangle = \frac{1}{\sqrt{2}}(\|H\rangle - i\|V\rangle)$	$\frac{1}{\sqrt{2}}\begin{pmatrix}1\\-i\end{pmatrix}$
left-hand circular	$\|L\rangle = \frac{1}{\sqrt{2}}(\|H\rangle + i\|V\rangle)$	$\frac{1}{\sqrt{2}}\begin{pmatrix}1\\i\end{pmatrix}$

Optical element (fast axis w.r.t. horizontal axis)	Jones matrix
HWP@0°	$e^{-\frac{i\pi}{2}}\begin{pmatrix}1&0\\0&-1\end{pmatrix}$
HWP@45°	$e^{-\frac{i\pi}{2}}\begin{pmatrix}0&1\\1&0\end{pmatrix}$
QWP@0°	$e^{-\frac{i\pi}{4}}\begin{pmatrix}1&0\\0&i\end{pmatrix}$
QWP@90°	$e^{\frac{i\pi}{4}}\begin{pmatrix}1&0\\0&-i\end{pmatrix}$

where λ_0 is the vacuum wavelength of the light. The most common wave plate designs include the so-called half-wave plate (HWP) and quarter-wave plate (QWP). These retarders impose relative phases $\Gamma = \pi$ and $\Gamma = \frac{\pi}{2}$ between polarizations along their fast and slow optical axis respectively.

In optics, change in polarization can be described using the Jones calculus, where polarized light is represented by a Jones vector and optical elements such as wave plates are represented by matrices (see Table 2.1). The action of an optical element on a polarized light is then calculated by applying corresponding matrix to a Jones vector.

2.4.5 Interference filter

As it was discussed in previous Section 2.3, the photons for QIP are often required to be indistinguishable in several characteristics. The indistinguishability in wavelengths among involved photons is achieved by spectral filtering often realized by interference filters.

The construction of bandpass interference filter is modeled after a Fabry-Perot interferometr which consists of two partially transparent mirrors separated by an air gap [75]. The principle of wavelength selection relies on the interference of multiple reflected beams inside the resonator. It is evident that the construction ensures an even number of reflections for the transmitted waves. If there is no phase difference between emerging waves the interference is constructive, therefore, the transmission is maximal. This is dependent on the optical path difference which for maximal transmission should be integral multiple of the desired wavelength. The constructive interference condition allows the central wavelength of the resonator together with small bend of wavelengths to either side, to be transmitted effectively. The FWHM (full width at half maximum) of the transmission peaks is influenced by reflectance of the mirrors, where higher reflectance produces narrower peaks [76]. Wavelengths that do not obey this condition are suppressed by destructive interference and thus reflected toward a source. However, the blocked bands around the central wavelength are quite narrow. It is due to other allowed wavelengths that meet the condition and the reduced reflectance outside the central wavelength. In order to broaden the range of blocked wavelengths, materials with wide absorption spectra (e.g., colored glass filters) should be part of the interference filter.

In commercially available bandpass interference filters the air gap is replaced by a dielectric spacer layer with optical thickness $n\frac{\lambda}{2}$, where n is a integer and λ the central wavelength[6], which can be made of colored glass to enhance the blocking range of the filter. The highly reflected mirrors are made of several stacks separated by the aforementioned spacer layer. The stacks are composed of a number of thin $(\frac{\lambda}{4})$ dielectric layers with alternating low and high indices of refraction. The assembly of a half-wave spacer layer sandwiched between two quarter-wave stacks is called a cavity. A bandpass interference filter can be formed by multiple of these cavities, where the advantages of multi-cavity filters are steeper band slopes and improved near-band rejection. Finally, the bandpass interference filters based on Fabry-Perot design are often designated for use at zero angle of incidence. This is because transmission band will be shifted in wavelength and might be reduced if other angle of incidence is used [77].

Theoretically any type of filter (low-pass, high-pass, band-pass, neutral density, etc.) can be constructed with this technique. In the presented experiments

[6] wavelength with the highest transmittance

narrow band-pass interference filters (IF) of FWHM 5 nm and 10 nm were used.

2.5 Quantum state analysis

As in many QIP schemes and all experiments presented in later chapters, the information is encoded into the state of single photons. Therefore, in order to read the information stored within the qubits one needs to perform a quantum state analysis and also be able to detect the individual photons.

There is a number of detectors that posses single-photon sensitivity. For instance, avalanche photo-diodes in Geiger mode, photomultipliers or array detectors such as iCCD (intensified CCD) and EM-CCD (electron multiplying CCD). There are also rather exotic single-photon detectors e.g., transition-edge sensors (TES) or nanowires. These detectors have excellent quantum efficiencies but require intensive cooling [78]. In hereby presented experiments silicon based avalanche photo-diodes in Geiger mode were used. The quantum efficiency for the near infrared wavelengths employed in the experiments was around 60%. Note that even though this type of detector is sensitive enough to detect individual photons, it is unable to resolve how many photons have actually been absorbed by the detector within the detection window. The photon number resolution can however be achieved by other types of detectors (e.g, TES) or by time or space multiplexing [74, 79]. A specially designed fiber loop that splits incoming optical pulse into a number of segments each containing ideally a single photon is an example of time multiplexing.

Note that in QIP schemes that include two or more photons instead of single-photon detections, the experimentalist records coincidence detections i.e., simultaneous detection events by two or more detectors.

The full quantum state analysis also know as quantum state tomography (QST) is required if one wishes to fully characterize the quantum state. The analysis consists of a number of repeated measurements designed to obtain enough data to reconstruct the density matrix. In the case of polarization encoding, these measurements are composed of all the mutual combinations of single photon polarization projections (i.e., $|H\rangle$, $|V\rangle$, $|D\rangle$, $|A\rangle$, $|R\rangle$, $|L\rangle$) implemented by polarizers and half- and quarter-wave plates. Then from the coincidence rates under various projections one can estimate the density matrix belonging to the initial quantum state. In our workflow, maximum likelihood algorithm is used to find such a physically valid density matrix that best fits the observed coincidence counts under the above-mentioned projection settings [80]. Note that in order to reveal or confirm some property (e.g, entanglement) of the quantum state one does not have to resort to QST. This is because the density matrix might contain more information then is required. Therefore, a subset of the projection measurements can be sufficient for the detection of the property. The reduction in the number

of measurements does not come for free. For instance, one needs to know some *a priori* information about the investigated quantum state or requires a second identical quantum state which interacts with the initial state.

2.6 Entanglement witness

Since 1935 when Einstein, Podolsky and Rosen published their seminal paper [81], the scientific community was caught in a dispute between the supporters and critics of quantum theory that lasts to this date. In the heart of the debate is the quantum mechanical principle of superposition that necessarily leads to the concept of quantum entanglement. Phenomenon that is frowned upon by the advocates of local realism who call it the "spooky action at a distance" [82, 83]. In 1964 John Bell created a theorem in which he expressed this philosophical dispute in a form of mathematical inequality

$$C_{\mathrm{h}}(a,c) - C_{\mathrm{h}}(b,a) - C_{\mathrm{h}}(b,c) \leq 1, \tag{2.19}$$

where C_h denotes correlations as predicted by local hidden variable (LHV) theories and a, b and c refer to three arbitrary measurement settings [84]. The inequality sets a upper bound on the quantum correlations between measurements preformed on a quantum system. LHV theories satisfy these inequalities for any quantum system. On the other hand quantum mechanics predicts for some systems violation of the inequalities. Experimental verification of the violation would state that nature can not be described by local realism and that quantum mechanics is complete. However experimental realization of the original Bell inequality was not applicable due to technical difficulties. Those issues were overcome by Clauser, Horne, Shimony and Holt who modified the Bell inequalities making experimental testing possible [85]. These modified inequalities are called CHSH inequalities and can be written as

$$|S| \leq 2, \tag{2.20}$$

where

$$S = E(a,b) - E(a,b') + E(a',b) + E(a',b'), \tag{2.21}$$

where a, a' and b, b' are measurement settings. The terms $E(a,b)$ represent quantum correlations between the particles. For further information see comprehensive review on Bell non-locality by Brunner *et al.* [86].

Instead of Bell inequality measurements which are used mainly for testing the theory of quantum mechanics in relation to the concepts of locality and realism, entanglement witnesses (EWs) are specifically tuned for the detection of entangled states. EWs are functionals of density matrices of investigated states and as such they are experimentally measurable quantities. Generally, an observable $\mathcal{W}$ is an

entanglement witness if its mean value is non-negative

$$\langle \mathcal{W} \rangle_{\hat{\rho}_{\text{sep}}} \geq 0 \tag{2.22}$$

for all separable states and negative

$$\langle \mathcal{W} \rangle_{\hat{\rho}_{\text{ent}}} < 0 \tag{2.23}$$

for at least one entangled state. For further information on the properties of entanglement witnesses see the excellent reviews [54, 87].

Entanglement witness is linear if it is a linear functional of density matrix or the mathematical expression of the witness does not include any non-linear terms of expectation values. In such case one needs to know some information about the investigated state to optimize performance of the witness.

There are also non-linear entanglement witnesses which can be further differentiated into two classes. First class being non-linear entanglement witnesses which add non-linear terms of expectation values to existing linear witnesses improving on the set of entangled states that can be detected [88–90]. Second class of non-linear entanglement witnesses are non-linear functionals of density matrix which also detect larger set of entangled states then linear witnesses but rely on joint measurements on multiple copies of an investigated state [91, 92]. For this reason they are known as collective entanglement witnesses (CEWs). Two of the experiments presented in later chapters employ a collective entanglement witness also known as collectibility, which was introduced by Rudnicki *et al.* [56, 57].

Chapter 3

Measurement of a non-linear entanglement witness by hyper-entangling two-qubit states

Text adopted from *Vojtěch Trávníček, Karol Bartkiewicz, Antonín Černoch, and Karel Lemr, Phys. Rev. A* ***98****, 032307 (2018)* [A3].

3.1 Introduction

There are two commonly used methods for entanglement characterization. The first method is based on quantum state tomography and density-matrix reconstruction [80, 93–95]. The advantage of this strategy is that one does not have to possess any *a priori* information about the input state. On the other hand, executing a full state tomography is a time demanding process especially for multi-level quantum states. The number of required measurements grows exponentially with the dimension of the investigated state which makes both the necessary measurement and the related data processing very time consuming [96].

The second method is based on the already mentioned entanglement witnesses (EWs). Measuring simple linear EWs requires performing a set of suitable local measurements which are direct products of projections applied on each subsystem separately. These projections are chosen based on some *a priori* information about the investigated state. Correlations of these local measurements across involved parties then reveal the entanglement [85].

The second class of EWs encompasses the non-linear (collective) entanglement witnesses [91, 97, 98] which removes the need for *a priori* information about a given state, but requires simultaneous measurements on at least two copies of the state. This idea has been experimentally demonstrated in a seminal paper by Bovino *et al.* [99]. In fact, a number of non-linear EWs [56, 57, 92, 100–106] have been devised for various classes of quantum states. Moreover, univer-

sal experimental optical approaches to measuring or detecting the entanglement of an arbitrary two-qubit state have been reported [107–109]. These universal approaches require using up to four copies of the state. With two copies only, the EWs are considerably easier to implement, but fail to detect some entangled states or require larger numbers of distinct measurements.

This chapter describes the benefits of entanglement detection by means of a non-linear EW on hyper-entangled states (HESs). A HES is a quantum state entangled in more than one degree of freedom (d.o.f.) and can be written in the form

$$\hat{\rho}_{\mathrm{HES}} = \hat{\rho}^{(\mathrm{p})} \otimes \hat{\rho}^{(\mathrm{s})}, \tag{3.1}$$

where subscripts p and s stand for two independent d.o.f. These states are an invaluable resource for quantum information protocols. They can be used for increasing channel capacity [110], efficient quantum key distribution [111], two-qubit teleportation [111], or serve as a powerful safeguard against eavesdropping [112]. Therefore, their quick detection and diagnosis is of paramount importance for practical implementation of the mentioned protocols. For instance, Bell state preparation and discrimination using hyper-entanglement was reported by Barbieri and co-workers [113, 114]. An EW on HESs was achieved by Walborn *et al.*, however, this witness operates only on pure states and their experimental setup cannot be simply modified to generate and test mixed states [100].

By hyper-entangling only a single photon pair instead of preparing multiple copies of a polarization-entangled pair of photons, we measure a non-linear EW on this single pair of hyper-entangled photons. For the purposes of demonstrating this concept, one of the less complex non-linear EWs known as the collectibility was selected [56, 57].

The original technique proposed by the authors of Refs. [56, 57] allows one to detect two-qubit entanglement in a large number of entangled states without the need for any *a priori* information about the investigated state. The collectibility measurement of two-qubit systems entangled in one d.o.f. requires to perform the collective measurements on two identical copies of the investigated state [58]. On the other hand collectibility can be measured directly on a single multilevel state where a two-qubit state is copied across two d.o.f. forming a HES. Generating two independent copies of a two-qubit state might seem easier, but properly managing their interaction is highly demanding even on the platform of linear optics. Note that in such case, ultrashort pumping together with narrow spectral filtering is required to assure proper synchronization [58, 97]. Further, a typical four-photon generation rate is about 10 mHz while with the hyper-entangled states of two photons, one obtains hundreds of events per second. The collective measurements of HESs consists of local and non-local projections. Local and non-local in this concept stand for projections implemented separately respectively across the two

d.o.f. This method of entanglement detection is tested on three characteristic two-qubit quantum states encoded twice into two separate d.o.f. of a photon pair. These states are Bell state, pure separable state, and maximally mixed state.

3.2 Theoretical framework

A hyper-entangled state is, e.g., a system composed of two quantum particles (subsystems A and B) each encoding two qubits, one qubit per d.o.f. A pair of photons with polarization (p) and spatial (s) d.o.f. is an example of such a system. For the purpose of our analysis we consider only identical states encoded into both d.o.f., i.e., $\hat{\rho}^{(\mathrm{p})} = \hat{\rho}^{(\mathrm{s})}$, where $\hat{\rho}^{(\mathrm{x})} = \hat{\rho}_{\mathrm{Ax,Bx}}$ for $\mathrm{x} = \mathrm{p}, \mathrm{s}$.

The collectibility of such system is defined in terms of five different local projections, where four of these projections are implemented simultaneously with one non-local projection [58]. One subsystem (A) of the HES is measured with separable projections, the other (B) with an entangled projection. The entanglement, in terms of collective non-linear entanglement witness $W(\hat{\rho})$, is then derived from correlations between coincidence rates observed for these projections. The correlations between coincidence rates of individual projections labeled p_{ij} can be expressed in terms of joint projection probabilities

$$p_{ij} = \mathrm{Tr}\left[\hat{\Pi}^{(i)}_{\mathrm{Ap}} \otimes \hat{\Pi}^{(j)}_{\mathrm{As}} \otimes \left(|\psi^-\rangle\langle\psi^-|\right)_{\mathrm{Bp,Bs}} \hat{\rho}_{\mathrm{HES}}\right]. \tag{3.2}$$

Indices Xp and Xs mark the relevant d.o.f. for subsystem $\mathrm{X} = \mathrm{A}, \mathrm{B}$, whereas indices $i, j = 0, 1, +$ represent projections on qubit states $|0\rangle$, $|1\rangle$, and $|+\rangle = (|0\rangle + |1\rangle)/\sqrt{2}$ expressed in the computational basis. The projection $(|\psi^-\rangle\langle\psi^-|)_{\mathrm{Bp,Bs}}$ stands for projecting the subsystem B onto a singlet state across the d.o.f. p and s, where

$$|\psi^-\rangle_{\mathrm{Bp,Bs}} = \tfrac{1}{\sqrt{2}}\left(|01\rangle - |10\rangle\right)_{\mathrm{Bp,Bs}}. \tag{3.3}$$

Using the notation from Ref. [58] and Eqs. (3.2), the collective non-linear entanglement witness can be formulated as

$$\begin{aligned} W(\hat{\rho}) = &\frac{1}{2}[\eta + P^2(1-p_{00}) + (1-P)^2(1-p_{11}) \\ &+ 2P(1-P)(1-p_{01}) - 1], \end{aligned} \tag{3.4}$$

where

$$\eta = 16P(1-P)\sqrt{p_{00}p_{11}} + 4p_{++}, \tag{3.5}$$

and $P = \mathrm{prob}(|0\rangle_{\mathrm{Ap}}) = \mathrm{prob}(|0\rangle_{\mathrm{As}})$ is the probability of observing subsystem A in state $|0\rangle_{\mathrm{Ap}}$ ($|0\rangle_{\mathrm{As}}$) independently of the state of subsystem B.

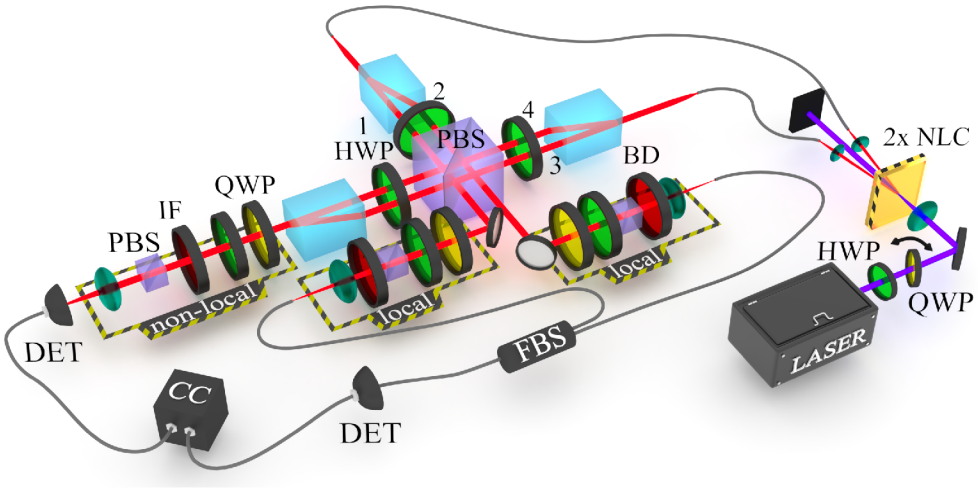

Figure 3.1: Experimental setup for measuring collectibility of photonic two-qubit states by hyper-entangling the input photons. BD: beam displacer; HWP: half-wave plate; PBS: polarization beam splitter; QWP: quarter-wave plate; IF: 10 nm interference filter; FBS: fiber beam splitter; DET: single-photon detector; CC: coincidence counter. Spatial modes are labeled by numbers 1-4.

3.3 Experimental implementation

The experimental implementation was realized on a platform of linear optics with a hyper-entangled pair of photons encoding the same two-qubit state in both polarization and spatial d.o.f. A horizontally polarized photon (i.e., subsystem $\mathrm{X} = \mathrm{A}, \mathrm{B}$) encodes the logical state $|0\rangle_{\mathrm{Xp}}$, a vertically-polarized photon state $|1\rangle_{\mathrm{Xp}}$. Similarly, spatial modes 1 and 3 encode logical state $|0\rangle_{\mathrm{As}}$ and $|0\rangle_{\mathrm{Bs}}$, modes 2 and 4 logical state $|1\rangle_{\mathrm{As}}$ and $|1\rangle_{\mathrm{Bs}}$. Thus, the relation between the states encoded in the computational basis and in the states used in the experiment can be expressed as

$$\begin{aligned} |mn\rangle_{\mathrm{Ap,As}} &\equiv |\delta_{m,1}V + \delta_{m,0}H\rangle_{1+n} \\ |kl\rangle_{\mathrm{Bp,Bs}} &\equiv |\delta_{k,1}V + \delta_{k,0}H\rangle_{3+l}, \end{aligned} \tag{3.6}$$

where δ stands for the Kronecker's delta, indices $m, k = 0, 1$ mark the single-photon polarization states, and indices $n, l = 0, 1$ the spatial modes $1 + k$ and $3 + l$.

The experimental setup consists of a two–photon source powered by pulsed Paladine (Coherent) laser at $\lambda = 355\,\mathrm{nm}$ with 300 mW of mean optical power and repetition rate of 120 MHz.

Polarization-entangled photon pairs at $\lambda = 710\,\mathrm{nm}$ are generated in non-collinear type I spontaneous parametric down-conversion (SPDC) process in a BBO (β-BaB_2O_4) crystal cascade (known as the Kwiat source [73]). This type of light source if pumped by a generally polarized pumping beam generates pairs of

horizontally and vertically polarized photons. Generation rates of these photons as well as their mutual phase shift can be tuned by adjusting the polarization of pumping beam. This way one can prepare states with various amount of entanglement. Each photon from the generated pair is coupled into a single-mode optical fiber and brought to one input port of the experimental setup depicted in Figure 3.1.

The beam displacers (BD) transform polarization entanglement into spatial entanglement and the two photons can interact on a polarizing beam splitter (PBS) where they get entangled in polarization again. Thus, a given HES is prepared.

The HES is consequently subjected to separable and entangled polarization projective measurements. The photon leading to the detector through fiber beam splitter (FBS) is subjected to separable projections $\hat{\Pi}_{\mathrm{p}}^{(i)} \otimes \hat{\Pi}_{\mathrm{s}}^{(j)}$ for $i, j = 0, 1$ as described in section 3.2. For example projection $\hat{\Pi}_{\mathrm{Ap}}^{(0)} \otimes \hat{\Pi}_{\mathrm{As}}^{(0)}$ corresponds to a projection onto a state $|00\rangle_{\mathrm{Ap,As}}$ or, by using Eq. (3.6), $|H\rangle_1$. The other photon is projected on state $|\psi^-\rangle_{\mathrm{Bp,Bs}}$ or equivalently [see Eqs. (3.3) and (3.6)] $\frac{1}{\sqrt{2}}(|H\rangle_4 - |V\rangle_3)$. Both projections are implemented by means of half-wave plates (HWP), quarter-wave plates (QWP) and polarizing cubes (PBS). The photons are then filtered by 10 nm interference filters (IF), coupled into single-mode optical fibers and brought to single-photon detectors. Motorized translations (not depicted) ensure temporal overlap of the photons on PBS and FBS.

3.4 Measurement and results

The collectibility was measured for three characteristic quantum states: (i) $|\psi_1\rangle = \frac{1}{\sqrt{2}}(|00\rangle + |11\rangle)$ (Bell state), (ii) $|\psi_2\rangle = |10\rangle$ (pure separable state), (iii) $\hat{\rho}_3 = \frac{1}{4}\hat{\mathbb{1}}$ (maximally mixed state), which were encoded twice in the following HESs

$$\begin{aligned} |\Psi_x\rangle_{\mathrm{HES}} &= |\psi_x\rangle_{\mathrm{Ap,Bp}} \otimes |\psi_x\rangle_{\mathrm{As,Bs}} \quad \text{for } x = 1, 2, \\ \hat{\rho}_{3,\mathrm{HES}} &= \tfrac{1}{16}\,\hat{\mathbb{1}}_{\mathrm{Ap,Bp,As,Bs}}. \end{aligned} \tag{3.7}$$

States (3.7) generated in the experiment can be expressed via Eq. (3.6) as

$$\begin{aligned} |\Psi_1\rangle_{\mathrm{HES}} &= \tfrac{1}{2}(|HH\rangle_{1,3} + |HH\rangle_{2,4} + |VV\rangle_{1,3} + |VV\rangle_{2,4}) \\ |\Psi_2\rangle_{\mathrm{HES}} &= |VH\rangle_{2,3}, \\ \hat{\rho}_{3,\mathrm{HES}} &= \tfrac{1}{16}\,\hat{\mathbb{1}}^{(\mathrm{p})} \otimes \hat{\mathbb{1}}^{(\mathrm{s})}. \end{aligned} \tag{3.8}$$

In order to prepare the state $|\Psi_1\rangle_{\mathrm{HES}}$, one needs to set the pumping beam polarization to diagonal orientation, rotate HWPs in front of the PBS to 22.5° w.r.t. horizontal axis and ensure the photon overlap on PBS. The state $|\Psi_2\rangle_{\mathrm{HES}}$ was prepared by setting the pump beam to horizontal polarization, therefore, only

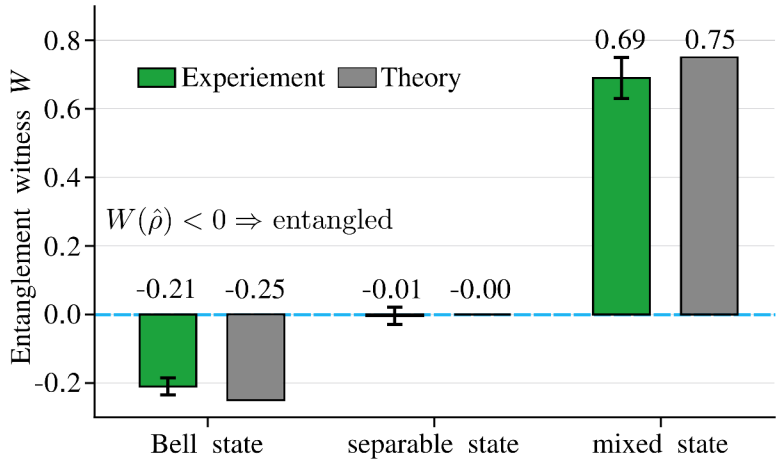

Figure 3.2: Experimental results and theoretical values of entanglement witness for three characteristic quantum states. Note that measurement values are in good agreement with the theoretically predicted values. As expected, the witness gives a clearly negative values only in the case of the Bell state.

Table 3.1: Measured values of collectibility W and its theoretical predictions W_{th} obtained for the states defined in Eq. (3.8).

Quantum state	W	W_{th}
Bell state ($\|\Psi_1\rangle_{\text{HES}}$)	-0.21 ± 0.03	-0.25
Separable state ($\|\Psi_2\rangle_{\text{HES}}$)	-0.01 ± 0.03	0.00
Mixed state ($\hat{\rho}_{3,\text{HES}}$)	0.69 ± 0.06	0.75

one of the BBO crystals was capable of dawn conversion, generating pairs of vertically polarized photons. Then by rotating a HWP (not depicted) in front of the beam displacer (BD) to 45°, one prepares the state $|VH\rangle_{2,3}$. In the case of the state $\hat{\rho}_{3,\text{HES}}$, which was not prepared directly, the outcome of each projection was obtained by accumulating coincidence rates associated with four Bell states.

For the Bell and mixed state, the probability P was set to $P = 0.50$, and for the separable state to $P = 0.01$. The values of P are adjusted using purely single-photon detection events and as a result the uncertainties of P are negligible in comparison with the uncertainty of two-photon coincidence detections. Obtained experimental and theoretically calculated values of collectibility $W(\hat{\rho})$ for the states from (3.8) are summarized in Table 3.1 and visualized in Figure 3.2.

Further, we have investigated the collectibility of Werner states which up to local unitary transformations can be expressed in the form of a weighted sum of maximally entangled and maximally mixed state,

$$\hat{\rho}_{\text{W}} = p|\Psi_1\rangle\langle\Psi_1| + q\hat{\rho}_3, \tag{3.9}$$

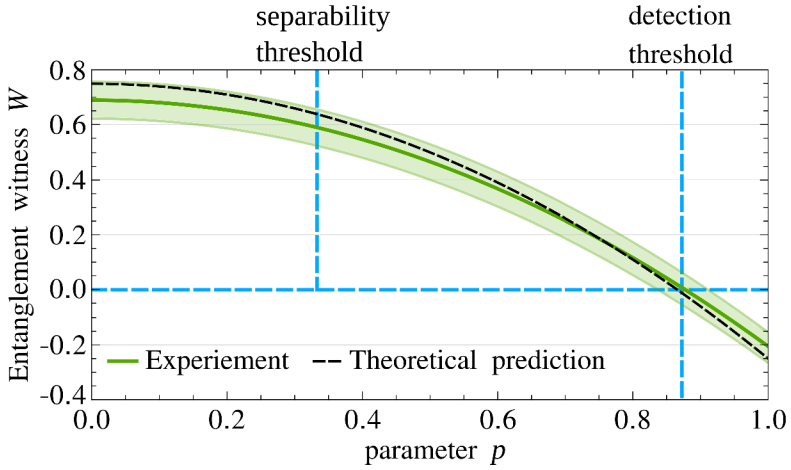

Figure 3.3: Experimental results and theoretical prediction of collectibility for the Werner states as a function of parameter p. The solid green line depicts the observed experimental results, the dashed black line is the theoretical prediction and the light green area corresponds to the measurement uncertainty.

where $0 \leq p \leq 1$ and $q = 1 - p$. It follows from Eq. (3.9) that p^2 (q^2) is the probability of observing the maximally entangled (mixed) state simultaneously in both d.o.f. The cross probability $2pq$ corresponds to observing entangled state in one d.o.f. and mixed state in the other d.o.f. It can be directly shown that for a mixed state encoded into one d.o.f., the projection probabilities p_{ij} and p_{++} are independent of the state encoded into the other d.o.f. As a consequence, to obtain the values of collectibility for Werner states, one can simply interpolate the results for $|\Psi_1\rangle$ and $\hat{\rho}_3$ with effective weights of p^2 and $1 - p^2$, respectively [58]. Note that the collective entanglement witness is able to detect entanglement only for $p > \frac{\sqrt{3}}{2}$ although Werner states are already entangled for any $p > \frac{1}{3}$ [58, 97, 99, 115]. Obtained experimental and theoretical values of collectibility $W(\hat{\rho})$ as a function of the parameter p are summarized in Table 3.2 and visualized in Figure 3.3.

In the experiment, collectibility of Werner states has been measured by properly combining (adding with proper weights) coincidence counts corresponding to three configurations of the setup: (i) the triplet state $|\Psi_1\rangle$, (ii) the mixed state $\frac{1}{2}(|01\rangle\langle 01| + |10\rangle\langle 10|)$ in both polarization and spatial modes and (iii) the mixed state $\frac{1}{2}(|00\rangle\langle 00| + |11\rangle\langle 11|)$ again in both polarization and spatial modes. In case of the triplet state $|\Psi_1\rangle$ positions of motorized translations were set so that the photons interfere on PBS and FBS. In case of the mixed states these translations have been deliberately detuned so that the photons become distinguishable and hence would not interfere. To switch between generation of the (ii) and (iii) state, we have used a half-wave plate inserted into spatial modes 1 and 2 behind the PBS together with relabeling of modes $3 \leftrightarrow 4$. Note that our experimental setup

Table 3.2: Assorted results obtained for Werner states defined in Eq. (3.9), where W is the observed value of entanglement witness and W_{th} is its theoretical prediction.

p	W	W_{th}
0.0	0.69 ± 0.06	0.75
0.2	0.65 ± 0.06	0.71
0.4	0.55 ± 0.06	0.59
0.6	0.37 ± 0.06	0.39
0.8	0.11 ± 0.06	0.11
1.0	-0.21 ± 0.03	-0.25

allows to directly generate mixed states of the form of

$$\begin{aligned} \hat{\rho}_4 &= p|\Psi_1\rangle\langle\Psi_1| + (1-p)|\Psi_5\rangle\langle\Psi_5| \text{ with} \\ |\Psi_5\rangle &= \tfrac{1}{2}(|HH\rangle_{1,3} - |HH\rangle_{2,4} - |VV\rangle_{1,3} + |VV\rangle_{2,4}). \end{aligned} \tag{3.10}$$

The parameter p is tuned by deliberate misplacement of the translations. This makes the photons partially distinguishable and thus the resulting state partially mixed.

3.5 Quick quality check of HES

Here, we demonstrate that collectibility can be used to quickly check the quality of hyper-entanglement. HES transmission through a noisy channel can result in decreased purity independently in both d.o.f. (i.e., in general $\hat{\rho}^{(\text{p})}$ and $\hat{\rho}^{(\text{s})}$ are different). This effect non-trivially affects the collectibility measurement. We obtained $\hat{\rho}^{(\text{p})}$ and $\hat{\rho}^{(\text{s})}$ states of different purities experimentally by intentionally detuning temporal overlap between the photons using motorized translations. The purity of the tested states does not affect the values of p_{ij} [see Eq. (3.2)] that corresponds to local projections onto states $|H\rangle_{1(2)}, |V\rangle_2$ [see Eq. (3.6)]. The only difference is observed for p_{++} which is measured by local projection $\frac{1}{2}(|H\rangle_1 + |V\rangle_1 + |H\rangle_2 + |V\rangle_2)$. Due to interference, this measurement is sensitive to phase difference between spatial modes 1 and 2. We define the ratio R as function of this phase shift,

$$R = \frac{cc_{\max}}{cc_{\min}}, \tag{3.11}$$

where $cc_{\max}$ and $cc_{\min}$ stand for maximum and minimum coincidences rates. The measurement was implemented by combining pure and mixed states $\hat{\rho}^{(\text{p})}$ with pure and mixed states $\hat{\rho}^{(\text{s})}$. The observed experimental values are summarized in Table 3.3 and visualized in Figure 3.4.

Table 3.3: Measured values of entanglement witness W and its theoretically predicated values W_{th} for the quality analysis of HESs for Werner states.

$\rho_{\text{W}}^{(\text{p})}$	$\rho_{\text{W}}^{(\text{s})}$	W	W_{th}
pure	pure	-0.21 ± 0.03	-0.25
pure	mixed	0.71 ± 0.06	0.75
mixed	pure	0.70 ± 0.06	0.75
mixed	mixed	0.69 ± 0.06	0.75

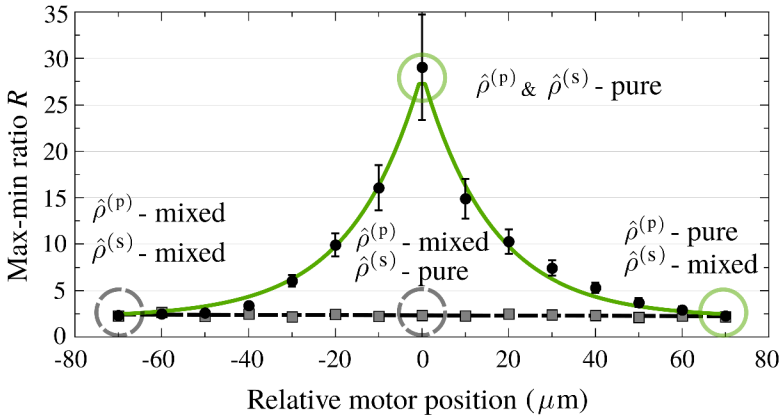

Figure 3.4: Experimental values of the ratio R [see Eq. (3.11)] obtained for the quality analysis of HESs for Werner states. The solid green (dashed black) curve corresponds to the fitting. Note that $R \to \infty$ for ideal experimental conditions. The collectibility has been measured for the encircled states.

Note that if a HES becomes disentangled in one d.o.f., the ratio R goes to 1 (as seen in Figure 3.4). The value of p_{++} is then $\frac{1}{4}$ and $W(\hat{\rho})$ is positive. On the other hand, when both $\hat{\rho}^{(\text{p})}$ and $\hat{\rho}^{(\text{s})}$ are sufficiently pure and entangled, $W(\hat{\rho})$ becomes negative. Hence, this method is a quick and easy way to diagnose HES distribution.

3.6 Conclusions

We have reported on experimental measurement of collective non-linear entanglement witness known as the collectibility on a single copy of a HES. The obtained results are in good agreement with theoretical predictions. The collectibility witness for hyper-entangled Bell state (-0.21 ± 0.03) is negative with sufficient certainty and also close to its theoretical value. As expected, the observed results of $W(\hat{\rho})$ for the separable and mixed state are non-negative and within one standard deviation from theoretically calculated values. We have interpolated the collectibility witness for several Werner states. These experimental results con-

form with theoretically predicted connection between collectibility witness and the Werner states parameter p. The method for diagnostics of HESs developed in this experiment is not as robust (fails on some partially entangled states) as quantum state tomography but can be appealing for applications that need fast verification whether the quantum system is sufficiently hyper-entangled. The experimental accessibility of our method makes it suitable for further development of other non-linear EWs requiring more than two copies of the measured state [107–109] or it can be easily adapted to measure a class of two-copy based EWs studied in Ref. [97]. The experience based on the currently presented experiment and the experiments implemented on two independent photon pairs [58, 97] shows that it is of similar difficulty to assure preparation of two identical two-qubit states in both cases. In the presented experiment, it was however much easier to implement mutual interaction between these states.

Chapter 4

Measurement of the Hilbert-Schmidt distance between two-qubit states

Text adopted from *Vojtěch Trávníček, Karol Bartkiewicz, Antonín Černoch, and Karel Lemr, Phys. Rev. Lett.* ***123****, 260501 (2019)* [A1].

4.1 Introduction

In quantum communications the quality of a transmission channel is crucial. It is due to security reasons, where imperfections of the communication channel lead to signal degradation known as noise. This noise can be subsequently exploited by potential eavesdroppers [116, 117]. Therefore, tools for the diagnostics of the transmission channels are in demand. In quantum communications theory one can quantify the accuracy of a signal transmission by measuring the distance in the Hilbert space between the transmitted and received states. The most prominent distance measures include the Uhlmann-Jozsa fidelity (Bures metrics), trace distance, and the Hilbert-Schmidt distance (HSD) (for overviews, see, e.g., [59, 60, A2].

These distance measures are also essential for a field of quantum machine learning. Where a common method for classification algorithms (e.g., k-means) is to perform a distance measurement among M sample vectors of dimension N. This procedure is a core subroutine for other machine learning algorithms, e.g., supervised and unsupervised nearest-neighbor algorithms. Quantum machine learning emerges as a new field of research in quantum information processing with linear optics, where the benefits of applying this platform are unaffected by unavoidably non-deterministic implementation of a universal set of gates [118]. It has been already demonstrated that by using quantum resources one can reduce the complexity of the k-means algorithm from $\mathcal{O}[\text{poly}(MN)]$ to $\mathcal{O}[\log(MN)]$ [42,

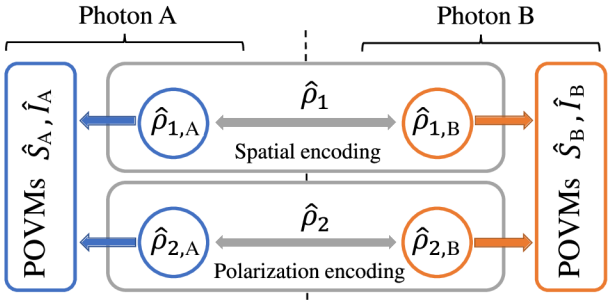

Figure 4.1: Conceptual scheme for measuring the Hilbert-Schmidt distance between two-qubit states. In general two different states $\hat{\rho}_1$ and $\hat{\rho}_2$ are encoded into polarization and spatial modes of photon A and B respectively. Photons A and B are then simultaneously measured by POVMs $\hat{I}$ and $\hat{\mathrm{S}}$, where the two degrees of freedom are addressed holistically at the same time. The operators $\hat{I}$ and $\hat{S}$ are the identity and singlet state projection where $\hat{S} = |\Psi^-\rangle\langle\Psi^-|$.

44, 118]. It was also shown in Ref. [A1] that by measuring the distance between a pair of points in terms of HSD one obtains the complexity of the distance-measuring algorithm $\mathcal{O}[\log(N)]$ by using a different approach from that in Ref. [44].

The HSD is defined as

$$D_{\mathrm{HS}}(\hat{\rho}_1, \hat{\rho}_2) \equiv \sqrt{\mathrm{Tr}[(\hat{\rho}_1 - \hat{\rho}_2)^2]}, \tag{4.1}$$

where $\hat{\rho}_1$ and $\hat{\rho}_2$ are the density matrices representing the two quantum, in general mixed, states. The HSD is a Riemann metrics, which makes it appropriate for applying in machine learning problems. Moreover, in contrast to trace distance, HSD is non-increasing under decoherence [59, 60]. For D-dimensional Hilbert space a density matrix contains $(D^2 - 1)$ independent parameters. This fact makes the complete quantum state tomography a very challenging problem, as it requires an exponentially large number of measurements in relation to the number of qubits constituting the composite system (see, e.g., [42, 94, 119]). However, this otherwise problematic feature also opens a new possibility to encode $N = D^2 - 1$ parameters in a D-dimensional density matrix (i.e., the Hilbert-Schmidt space). Note, that for pure states the number of independent parameters is much lower, i.e., $N = 2D - 1$. In this way, by using mixed instead of pure states one can encode quadratically more features into a given state. Once the encoding is performed for M states a constant number of times, each distance can be measured in only three steps. This is because the HSD can be expressed by first-order overlaps $O(\hat{\rho}_i, \hat{\rho}_j)$ as described in Refs. [120, 121] [A2]

$$D_{\mathrm{HS}}(\hat{\rho}_1, \hat{\rho}_2) = \sqrt{O(\hat{\rho}_1, \hat{\rho}_1) + O(\hat{\rho}_2, \hat{\rho}_2) - 2O(\hat{\rho}_1, \hat{\rho}_2)}, \tag{4.2}$$

where the directly measured observables are defined as $O(\hat{\rho}_i, \hat{\rho}_j) = \mathrm{Tr}(\hat{\rho}_i \hat{\rho}_j)$.

4.1.1 Two-photon overlap

The density matrix of a single qubit can be expressed using Bloch representation and making use of Einstein summation convention as (see. Ref. [122])

$$\hat{\rho} = \tfrac{1}{2} R_{m0} \hat{\sigma}_m, \tag{4.3}$$

where

$$R_{m0} = \mathrm{Tr}(\hat{\rho}\hat{\sigma}_m) \tag{4.4}$$

are elements of the Bloch vector defined by Pauli matrices $\hat{\sigma}_m$ $(m = 0, 1, 2, 3)$, where $\hat{\sigma}_0 = \hat{I}$ is the identity operator. The density matrix for two-qubit system can be written in the similar way as

$$\hat{\rho} = \tfrac{1}{4} R_{mn} \hat{\sigma}_m \otimes \hat{\sigma}_n, \tag{4.5}$$

where

$$R_{mn} = \mathrm{Tr}[\hat{\rho}(\hat{\sigma}_m \otimes \hat{\sigma}_n)] \tag{4.6}$$

are elements of the correlation matrix and $m, n = 0, ..., 3$. Then the first-order overlap defined as

$$O(\hat{\rho}_1, \hat{\rho}_2) = \mathrm{Tr}(\hat{\rho}_1 \hat{\rho}_2) \tag{4.7}$$

can be for two-qubit states calculated directly as

$$O(\hat{\rho}_1, \hat{\rho}_2) = \tfrac{1}{16} R^{(1)}_{mn} R^{(2)}_{kl} \mathrm{Tr}[(\hat{\sigma}_m \hat{\sigma}_n) \otimes (\hat{\sigma}_k \hat{\sigma}_l)] \tag{4.8}$$

where

$$R^{(1)}_{mn} = \mathrm{Tr}[(\hat{\sigma}_m \otimes \hat{\sigma}_n)\hat{\rho}_1], \tag{4.9a}$$
$$R^{(2)}_{mn} = \mathrm{Tr}[(\hat{\sigma}_m \otimes \hat{\sigma}_n)\hat{\rho}_2] \tag{4.9b}$$

are the correlation matrices of individual two-qubit states. Further form commutation and anti-commutation relations for the Pauli matrices one can compactly describe their multiplication as

$$\hat{\sigma}_i \hat{\sigma}_j = i\epsilon_{ijk}\hat{\sigma}_k + \delta_{ij}\hat{\sigma}_0, \tag{4.10}$$

where i is the imaginary unit, ϵ_{ijk} Levi-Civita symbol and δ_{ij} Kronecker delta. Because the Pauli matrices are traceless except of $\hat{\sigma}_0$ the trace of their multiplication is then

$$\mathrm{Tr}(\hat{\sigma}_m \hat{\sigma}_n) = 2\delta_{mn} \tag{4.11}$$

and the Eq. (4.8) simplifies to

$$O(\hat{\rho}_1, \hat{\rho}_2) = \frac{1}{4} R^{(1)}_{mn} R^{(2)}_{mn}. \tag{4.12}$$

Then by using Eqs. (4.9a,4.9b) one gets

$$\begin{aligned} O(\hat{\rho}_1, \hat{\rho}_2) &= \tfrac{1}{4}\mathrm{Tr}[(\hat{\sigma}_m \otimes \hat{\sigma}_n \otimes \hat{\sigma}_m \otimes \hat{\sigma}_n)(\hat{\rho}_1 \otimes \hat{\rho}_2)] \\ &= \tfrac{1}{4}\mathrm{Tr}[(\hat{\sigma}_m \otimes \hat{\sigma}_m) \otimes (\hat{\sigma}_n \otimes \hat{\sigma}_n)(\hat{\rho}_1 \otimes \hat{\rho}_2)'] \\ &= \tfrac{1}{4}\mathrm{Tr}[(\hat{V}_{a_1 a_2} \otimes \hat{V}_{b_1 b_2})(\hat{\rho}_1 \otimes \hat{\rho}_2)'], \end{aligned} \tag{4.13}$$

where $\hat{V} = \hat{\sigma}_m \otimes \hat{\sigma}_m = 2\hat{I} - 4|\Psi^-\rangle\langle\Psi^-|$, $|\Psi^-\rangle$ is the singlet state, and $(\hat{\rho}_1 \otimes \hat{\rho}_2)' = \hat{\Sigma}_{a_2 b_1}(\hat{\rho}_1 \otimes \hat{\rho}_2)\hat{\Sigma}_{a_2 b_1}$, where $\hat{\Sigma}_{a_2 b_1} = \hat{I} \otimes \hat{\Sigma} \otimes \hat{I}$ is unitary matrix swapping modes b_1 and a_2. Within this framework it is possible to introduce the Hermitian overlap operator $\hat{O}$ measured on $\hat{\rho}_1 \otimes \hat{\rho}_2$, i.e,

$$\hat{O} = \hat{\Sigma}_{a_2 b_1} \hat{V}_{a_1 a_2} \hat{V}_{b_1 b_2} \hat{\Sigma}_{a_2 b_1}. \tag{4.14}$$

Measuring the purity or first-order overlap can be performed by measuring a product of two $\hat{V}$ operators that can be experimentally implemented within the framework of linear optics, this was shown in Ref. [122].

The product of $\hat{V}$ operators can be expressed in terms of the 4 POVMs as

$$|\hat{V}|^2 = 4\hat{I} \otimes \hat{I} - 8\hat{S} \otimes \hat{I} - 8\hat{I} \otimes \hat{S} + 16\hat{S} \otimes \hat{S}, \tag{4.15}$$

where $\hat{S} = |\Psi^-\rangle\langle\Psi^-|$.

If $\hat{\rho}_1 = \hat{\rho}_2$, one measures purity as discussed, e.g., in Refs. [58, 99, 122]. Each overlap or other functions of overlaps can be measured directly by utilizing multiparticle interactions between copies of the investigated states [A2, 97, 120, 122–126]. In contrast, by applying full quantum tomography (see, e.g., [127]) $(D^2 - 1)$ measurements are required to calculate the value of HSD. For technical reasons we measure each overlap by utilizing four positive-valued measures (POVMs). For $D = 4$ this amounts to 12 POVMs for obtaining a single value of D_{HS}.

4.2 Experimental setup

This section describes the measurement of HSD in a linear-optical experiment with photons as information carriers. Here, the HSD is measured for two-qubit states by simultaneous interaction between four qubits. A straightforward approach uses four photons and only one degree of freedom (d.o.f.) such as polarization (see, e.g., Ref. [120]), however, this setup utilizes two d.o.f. (polarization and spatial) to encode two qubits (see Figure 4.1), therefore, only two photons were needed. This way one achieves much higher detection rates which make the experiment

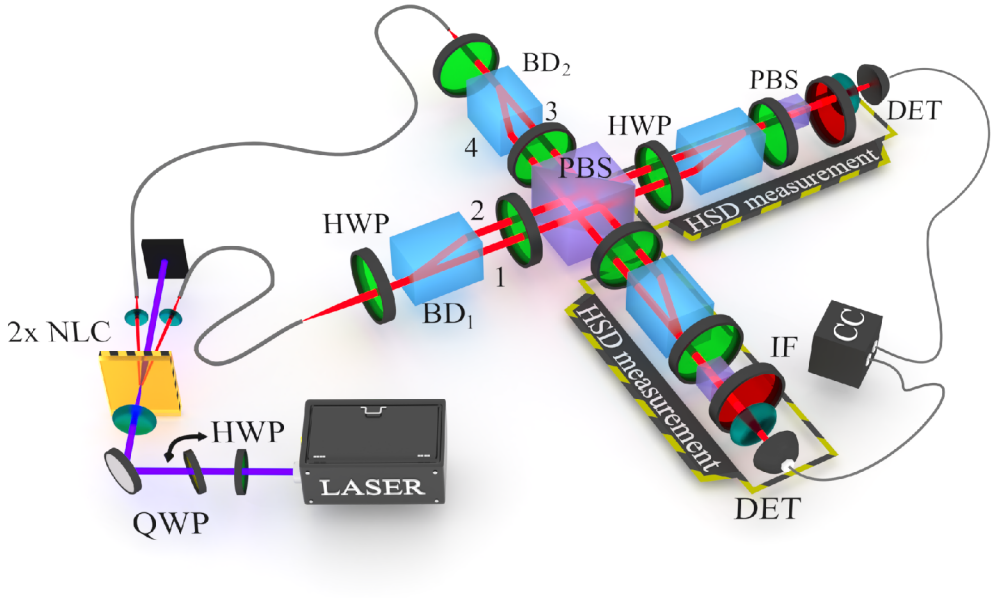

Figure 4.2: Experimental setup for measuring Hilbert-Schmidt distance between two two-qubit states. HWP: half-wave plate; BD: beam displacer; PBS: polarization beam splitter; QWP: quarter-wave plate; IF: 5 nm interference filter; DET: single-photon detector; CC: coincidence counter. Spatial modes are labeled by numbers 1-4.

considerably faster. The photons are labeled A and B, meanwhile their polarization and spatial modes are labeled p and s. There are horizontal (H) and vertical (V) polarization modes, and four spatial modes: 1-4 (see scheme in Figure 4.2). Horizontally polarized photons were associated with a logical state $|0\rangle$, vertically polarized photons with a logical state $|1\rangle$. Similarly, spatial modes 1 and 3 were associated with a logical state $|0\rangle$, modes 2 and 4 with a logical state $|1\rangle$. For example, photon A encodes state $|00\rangle$ if its polarization is made horizontal and it is placed in a spatial mode 1, i.e., in this notation $|H_1\rangle$.

The two photons are generated in a crystal cascade (known as the Kwiat source [73]) pumped by pulsed Paladine (coherent) laser a $\lambda = 355\,\text{nm}$ with 200 mW of mean optical power and a repetition rate of 120 MHz. The source consists of two BBO (β-BaB_2O_4) crystals and generates polarization-entangled photon pairs at $\lambda = 710\,\text{nm}$, i.e., $|\Psi\rangle = \cos(\alpha)|HH\rangle + e^{i\theta}\sin(\alpha)|VV\rangle$. The rates and mutual phase shift between horizontally and vertically polarized photons can be tuned by adjusting the pump beam polarization or by tilting one of the beam displacers (BD_1 or BD_2 in Figure 4.2). By doing so one can prepare states with various amounts of entanglement. Each photon from the generated pair is coupled into a single-mode optical fiber and brought to one input port of the experimental setup. The photons then pass through beam displacers where the initial polarization encoding is transformed into spatial encoding. Afterwards the photons interact on

the polarizing beam splitter (PBS) where a second, in principle different, quantum state is encoded into polarization d.o.f. As a result, two, in principle different, two-qubit states are encoded into the two d.o.f. The two states are then subjected to projective measurements (discussed below) and accompanied by postselection. The photons are filtered by 5 nm interference filters, coupled into single-mode optical fibers and brought to single-photon detectors. Motorized translation (not depicted) ensures temporal overlap of the photons on PBS. To demonstrate the versatility of this approach, the HSD was measured between four Bell states, four separable states, Werner states, and between Werner and Horodecki states.

To measure the HSD between any two states $(\hat{\rho}_1, \hat{\rho}_2)$ the first-order overlap has to be measured in three configurations, i.e., $O(\hat{\rho}_1, \hat{\rho}_1)$, $O(\hat{\rho}_2, \hat{\rho}_2)$ and $O(\hat{\rho}_1, \hat{\rho}_2)$. The first two configurations correspond to the situation when $\hat{\rho}_1$ ($\hat{\rho}_2$) is encoded into both d.o.f. During the last configuration $\hat{\rho}_1$ and $\hat{\rho}_2$ are encoded each in one d.o.f. Measurement of each first-order overlap $O(\hat{\rho}_1, \hat{\rho}_2)$ is split into a measurement of 4 POVMs on each photon across its d.o.f., i.e., $\hat{I}_\mathrm{A} \otimes \hat{I}_\mathrm{B}$, $\hat{S}_\mathrm{A} \otimes \hat{I}_\mathrm{B}$, $\hat{I}_\mathrm{A} \otimes \hat{S}_\mathrm{B}$, and $\hat{S}_\mathrm{A} \otimes \hat{S}_\mathrm{B}$,where the $\hat{I}$ stands for identity and the $\hat{S}$ for singlet state projection that were implemented by suitable rotation of half-wave plates (HWP) behind the PBS. For example, the POVM $\hat{I}_\mathrm{A} \otimes \hat{I}_\mathrm{B}$ consists of all combinations of local projections, i.e., $|H_1, H_3\rangle_{A,B}, |H_2, H_3\rangle_{\mathrm{A,B}}, ..., |V_2, V_4\rangle_{\mathrm{A,B}}$, while the $\hat{S}_\mathrm{A} \otimes \hat{S}_\mathrm{B}$ consists of projections $\frac{1}{\sqrt{2}}(|H_2\rangle - |V_1\rangle)_\mathrm{A}$ and $\frac{1}{\sqrt{2}}(|H_4\rangle - |V_3\rangle)_\mathrm{B}$. Both of these POVMs $(\hat{I}, \hat{S})$ can be implemented in a single step, but in this experiment they were implemented as a series of von Neumann projections. The coincidence rates corresponding to specific POVMs are labeled $f_{\hat{x}\hat{y}}$, where $\hat{x}, \hat{y} \in \{\hat{I}, \hat{S}\}$, where $\hat{x}$ and $\hat{y}$ are associated with photon A and B, respectively. These values are obtained by summing up the coincidence rates associated with respective von Neumann projections. The mean value of the overlap operators relates to these rates as

$$O(\hat{\rho}_1, \hat{\rho}_2) = 1 - 2(f_{\hat{S}\hat{I}} + f_{\hat{I}\hat{S}} - 2f_{\hat{S}\hat{S}})/f_{\hat{I}\hat{I}}. \tag{4.16}$$

Note that POVMs associated with $f_{\hat{I}\hat{I}}$ measures photon rate and is needed for normalization. In case of a stable photon source and know setup parameters this value is constant and state-independent. The same is true for POVMs $\hat{I}_\mathrm{A}$ and $\hat{I}_\mathrm{B}$ separately.

4.3 Results

First, distances between four Bell states $|\Phi^\pm\rangle = \frac{1}{\sqrt{2}}(|00\rangle \pm |11\rangle)$ and $|\Psi^\pm\rangle = \frac{1}{\sqrt{2}}(|01\rangle \pm |10\rangle)$ have been measured. Encoding of the states into the d.o.f. was implemented by a suitable choice of pump beam polarization, rotation of the HWPs, and by tilting one of the beam displacers (BD_1). For instance, the state $|\Phi^+\rangle$ was encoded into the polarization and spatial modes by setting the HWPs in

Table 4.1: Settings of HWPs and beam displacer for the preparation of Bell states in polarization and spatial d.o.f. BD-max (BD-min) stands for maximization (minimization) of coincidence events during $\hat{S}_{\mathrm{A}} \otimes \hat{S}_{\mathrm{B}}$ projection by tilting one of the beam displacers. The term Switch (+) represents change in measurement basis of one of the HWPs immediately behind PBS ($0° \leftrightarrow 45°$).

	HWPs (front of BDs)	HWPs (front of PBS)	BD	Switch
$\|\Phi^+\rangle\|\Phi^+\rangle$	0°,0°	22.5°,22.5°	max	-
$\|\Phi^+\rangle\|\Phi^-\rangle$	0°,0°	22.5°,22.5°	min	-
$\|\Phi^-\rangle\|\Phi^-\rangle$	0°,0°	−22.5°,−22.5°	max	-
$\|\Psi^-\rangle\|\Phi^-\rangle$	0°,0°	−22.5°,−22.5°	max	+
$\|\Psi^-\rangle\|\Phi^+\rangle$	0°,0°	−22.5°,−22.5°	min	+
$\|\Psi^-\rangle\|\Psi^+\rangle$	0°,45°	−22.5°,−22.5°	max	-
$\|\Psi^-\rangle\|\Psi^-\rangle$	0°,45°	−22.5°,−22.5°	max	-
$\|\Psi^+\rangle\|\Psi^+\rangle$	0°,45°	22.5°,22.5°	max	+
$\|\Phi^+\rangle\|\Psi^+\rangle$	0°,45°	22.5°,22.5°	max	-
$\|\Phi^-\rangle\|\Psi^+\rangle$	0°,45°	−22.5°,−22.5°	min	-

front of the beam displacers to 0° w.r.t horizontal axis and HWPs in front of PBS to 22.5°. Also BD_1 was tilted so there was maximum coincidence events while projecting both photons on a singlet state ($\hat{S}_{\mathrm{A}} \otimes \hat{S}_{\mathrm{B}}$). For the preparation settings of other states see Table 4.1. We have decided to plot a second power of the HSD denoted D^2_{HS} so it is linear in terms of the physically measured quantities. The obtained experimental and theoretically calculated values of the second power of HSD between Bell states are shown in Figure 4.3(a). Next, we have measured the HSD between separable states $|00\rangle$, $|11\rangle$, $|01\rangle$ and $|10\rangle$. The obtained values are visualized in Figure 4.3(b). In the third part of the experiment, the values of D^2_{HS} between Werner states have been calculated. A Werner state can be up to local unitary transformation expressed in a form of a weighted sum of maximally entangled and maximally mixed state

$$\hat{\rho}_{\mathrm{W}} = p|\Phi^+\rangle\langle\Phi^+| + \tfrac{1}{4}(1-p)\hat{I}. \tag{4.17}$$

In the case of the mixed state, the outcome of each von Neumann projection was obtained by accumulating coincidence rates associated with four Bell states, i.e., making use of the identity $\hat{\rho}_1 \otimes \hat{\rho}_2 = \frac{1}{4}(|\Psi^+\rangle\langle\Psi^+| + |\Psi^-\rangle\langle\Psi^-| + |\Phi^+\rangle\langle\Phi^+| + |\Phi^-\rangle\langle\Phi^-|) = \frac{1}{4}\hat{I}\otimes\hat{I}$. Subsequently, the values of D^2_{HS} have been calculated for various values of the weight parameter p. The results are visualized in Figure 4.4(a). Finally, the D^2_{HS} between Werner and Horodecki states have been calculated. Horodecki states can be expressed in the form of a weighted sum of the maxi-

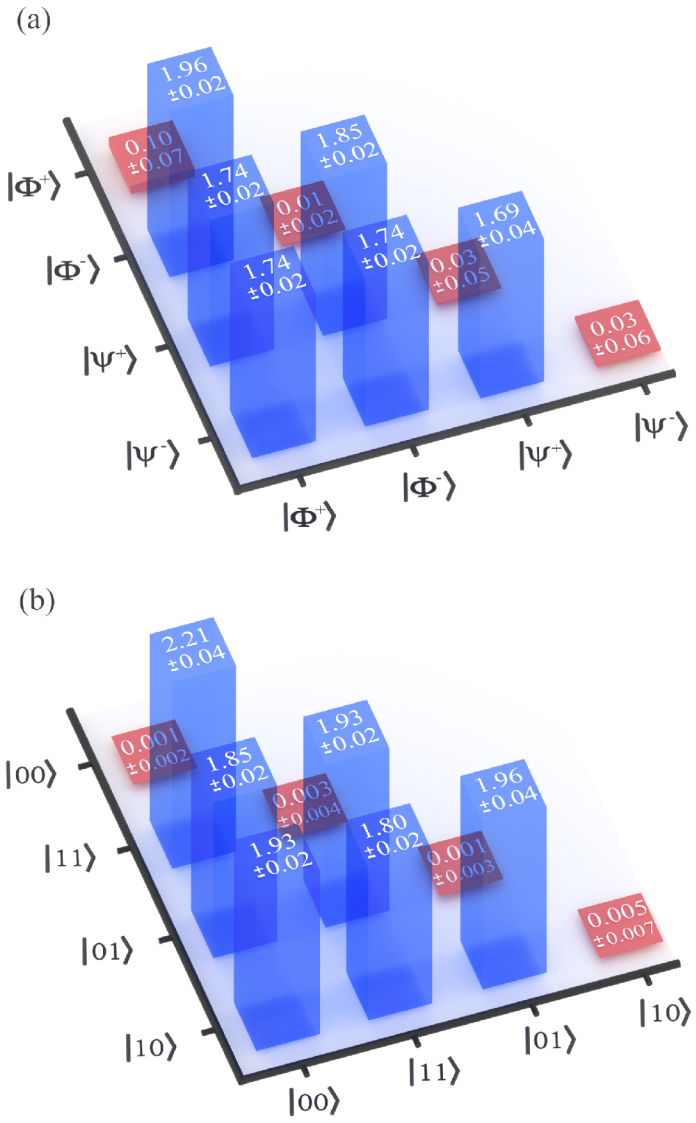

Figure 4.3: Experimental results of the second power of Hilbert-Schmidt distance D^2_{HS} between: (a) Bell states, (b) separable states. The axis represent polarization and spatial encoding (see Figure 4.1). Note that the theoretical value of the second power of Hilbert-Schmidt distance between identical states (situated in the diagonal) is 0, whereas D^2_{HS} reaches its upper theoretical limit of 2 between orthogonal states.

mally entangled and separable state

$$\hat{\rho}_{\mathrm{H}} = q|\Phi^-\rangle\langle\Phi^-| + (1-q)|01\rangle. \tag{4.18}$$

Therefore, one has to measure the overlap between states $|\Phi^+\rangle$ ($|\Phi^-\rangle$) and $|01\rangle$ encoded in polarization and spatial mode, respectively. The rest of the necessary overlaps were calculated in the same way as explained above. The values of D^2_{HS}

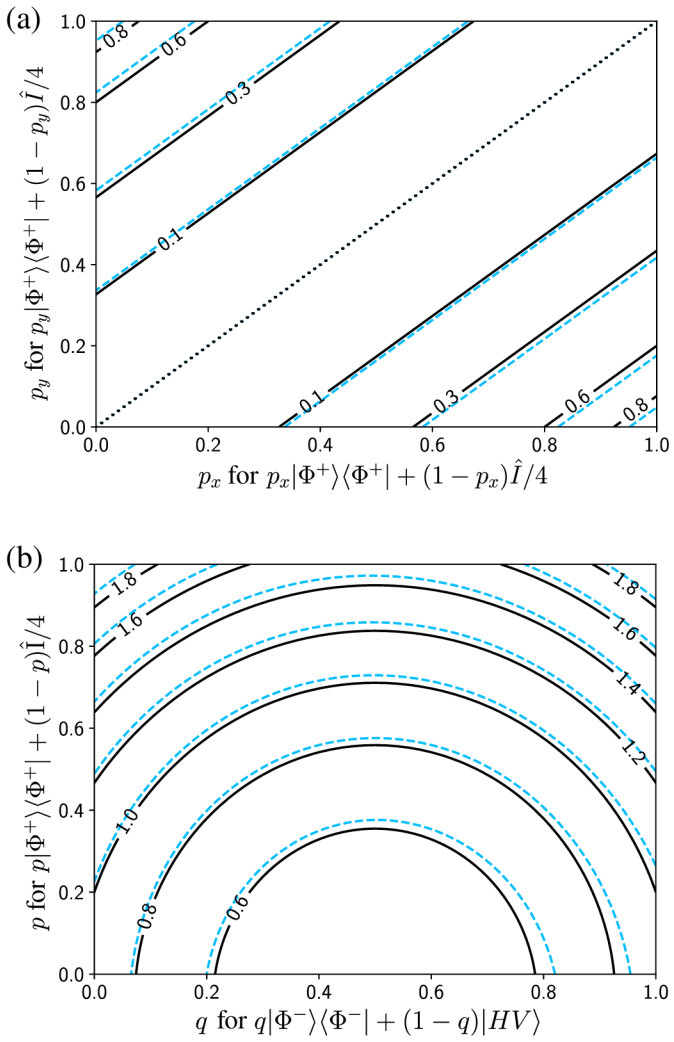

Figure 4.4: Experimentally obtained values of D^2_{HS} (a) between two Werner states and (b) between Werner and Horodecki states for various weight parameters $(p_{\mathrm{x}}, p_{\mathrm{y}})$ or (p, q) are represented by a corresponding light-shaded contours slightly shifted with respect to the labeled black contours representing the theoretical values of D^2_{HS}. The vertical and horizontal axis represent polarization and spatial encoding respectively (see Figure 4.1).

between Werner and Horodecki states for various weight parameters p and q are visualized in Figure 4.4(b).

4.3.1 Performance of the k-means algorithm

In order to analyze the impact of the measurement error on the performance of the k-means algorithm two numerical simulations were performed, where 2×10^4 points were divided into 2 clusters. These simulations calculated the distance between the points exactly or by introducing a relative error of 15% of the calculated distance. In the numerical simulations the points were sampled from two

Gaussian distributions of equal variance. The error in distance estimation results in approximately 4% (on average) of points being assigned to different clusters than assigned by the simulation with the exact distance calculation. The results of our simulations are summarized in Figure 4.5.

4.4 Conclusions

This work reports on the experimental measurement of the Hilbert-Schmidt distance between two-qubit states by the method of many-particle interference. The method allows to measure the HSD between two two-qubit density matrices by performing three overlap measurements (four POVMs per overlap). The scheme works for both mixed and pure states, however, using the former is more desirable for machine learning. This is because for a system of a fixed dimension D we can encode quadratically more features in a mixed state than in a pure state. This approach to measuring Euclidean distance between a pair of points in space of dimension $N = D^2 - 1$ exhibits a reduced complexity of $\mathcal{O}(\log N)$ in comparison to the standard approach of the complexity $\mathcal{O}(\text{poly}N)$. The obtained experimental results are in good agreement with theoretical predictions. To demonstrate the versatility of this approach HSD was measured between assorted two-qubit states. The HSD between identical Bell states is sufficiently close to theoretical values. On the other hand, distances between orthogonal Bell states do not deviate from theoretical values by more than 15%. This error is partially caused by the linearization of Eq. (4.1) and by phase instability in the relatively complex interferometer. Further, partial distinguishability between photons causes an imperfect bunching that leads to partial impurities of the states, therefore, increasing the error. However, this discrepancy is implementation specific and not a fundamental limit. To assess the impact of measurement errors on the shape of two clusters created using a k-means algorithm with and without introducing a maximum error of 15% in distance measurement we performed numerical simulations. The initial sets of points were created using Gaussian distributions (see [41]). The clusters created for the range of distances between the Gaussians varying from 0 to 6 standard deviations differ on average by 4% of the points. Similar measurement results were obtained for the separable states, however, the deviation from the theoretical prediction is not as high due to the lower complexity of the states. The HSDs between Werner states and between Werner and Horodecki states for various values of the weight parameters were also interpolated. The results are in good agreement with theoretical values represented by the contours in Figure 4.4. We believe that these results can motivate subsequent research on the topic of quantum channel characterization and quantum machine learning. Especially in the latter, measuring distances between multidimensional points efficiently can reduce the computational complexity of supervised and unsupervised

machine learning. Thus, the results can be inspiring for near term quantum technologies which would exhibit speedup in comparison to the best currently known classical solutions. The results are also a novel example of applying mixed states for quantum information processing. Usually working with mixed states is not desired, but here it gives the possibility of encoding extra information as the degree of coherence between the given two dimensions of the density matrix.

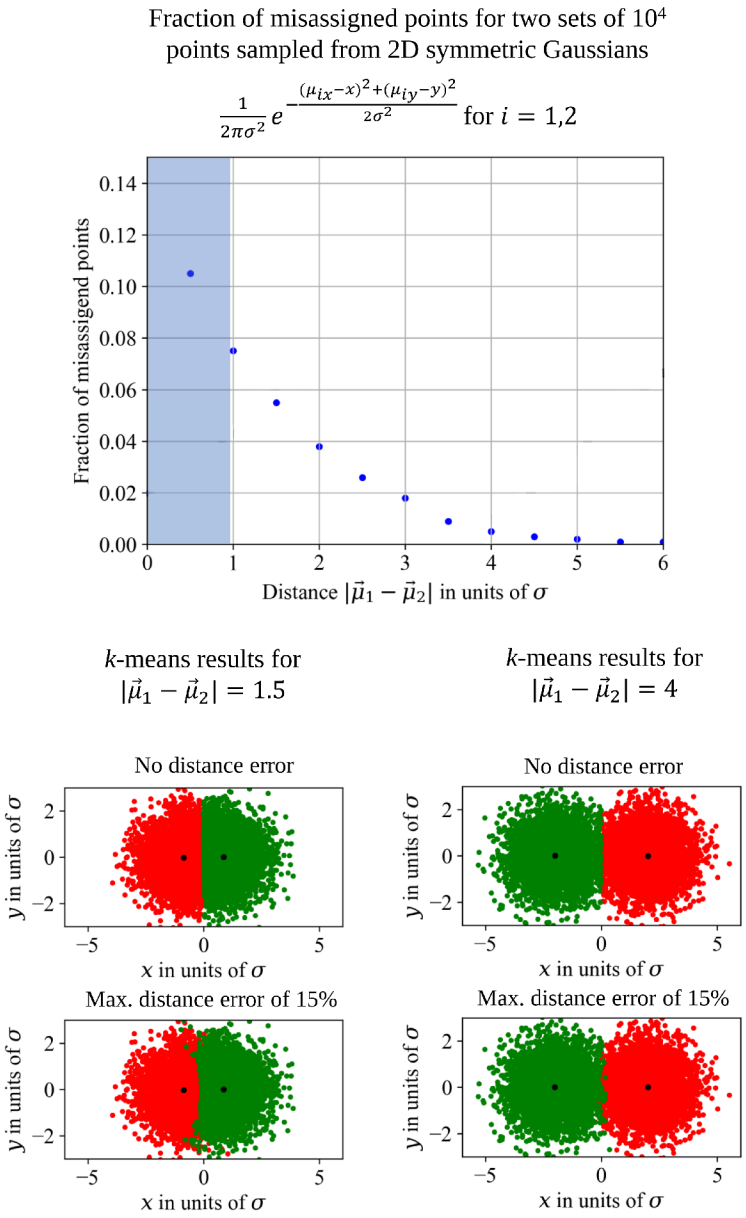

Figure 4.5: The influence of distance calculation errors on the performance of the k-means algorithm investigated by means of Monte-Carlo simulations. The k-means algorithm works best for finding symmetric clusters of similar size. Thus, the 2D points (in total 2×10^4) were selected to be divided into 2 clusters (clusters represented by dark green and red dots, and their centroids marked with black dots) by sampling from two 2D symmetric Gaussian distributions of equal variances (10^4 points per Gaussian). This way one can test the algorithm in the regime in which it performs correctly. The only variable is the distance between the central points (μ_1 and μ_2) of the Gaussians. The fraction of miss assigned clusters with and without accounting for the distance calculation errors is given in the central plot. Note that for the shaded range the average fraction is hard to estimate as the choice of the clusters for a finite number of points becomes more arbitrary with the distance between the Gaussians approaching 0. However, in this regime the numerically estimated average value was approximately 0.11.

Chapter 5

Diagnostics of entanglement swapping by a collective entanglement test

Text adopted from *Vojtěch Trávníček, Karol Bartkiewicz, Antonín Černoch, and Karel Lemr, Phys. Rev. Applied,* ***14****, 064071 (2020)* [A4].

5.1 Introduction

The exchange of quantum information between parties connected through a quantum network [35, 36] can become the inherently secure transmission of information [19, 20] or provide an improved transmission rate [110, 128]. However, none of the transmission media[1] is lossless which results in errors that influence the quality of the transmission. During quantum communications in free space the optical signal is attenuated due to geometrical losses such as diffraction and atmospheric extinction including absorption and scattering [129]. In an optical fiber the scaling of probability for a photonic qubit being absorbed, depolarized, or dephased grows exponentially with the length of the channel and remains the major obstacle to practical long-distance quantum communications [25]. This does not only restrict feasible lengths of quantum channels, but also represents a security threat as the errors could be exploited for a potential attack on the communication protocol [116, 117].

To combat these limitations, quantum repeaters and relays were proposed [25, 27]. Although the working principles of quantum repeaters and relays somewhat differ, they both operate by splitting the communication channel into segments, therefore, lowering the error probability. At their core, quantum repeaters and relays apply the entanglement-swapping (ES) protocol [26]. This involves teleportation of a quantum state of a particle that shares entanglement with at least

[1] e.g. optical fiber, free space (atmosphere)

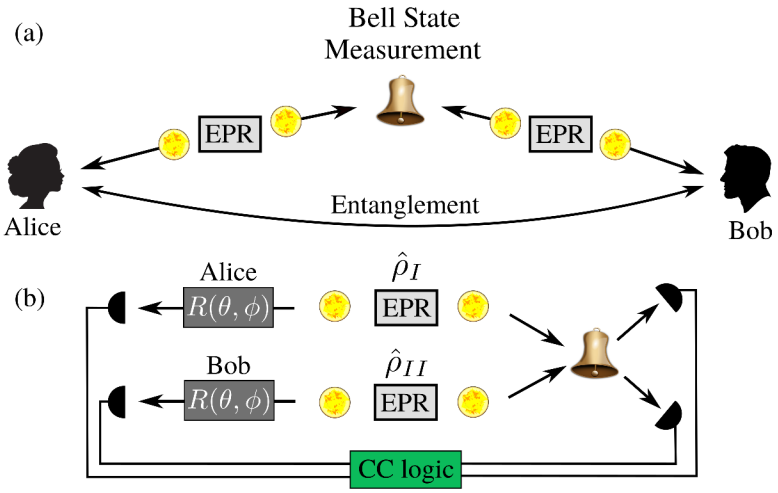

Figure 5.1: (a) Conceptual diagram of the ES protocol. Two entangled quantum states (e.g., two pairs of photons) are generated in EPR sources. One particle from each pair is subjected to a Bell-state measurement. This results in projecting the other two particles, which are sent to Alice and Bob, onto an entangled state. (b) Conceptual scheme for measurement of a CEW. To witness entanglement of a general two-qubit state $\hat{\rho}_I$, a copy $\hat{\rho}_{II}$ is prepared. Similarly to ES, one particle from each pair is subjected to a Bell-state measurement, while the remaining two particles are subjected to a set of individual local projections $R(\theta, \phi)$. The CEW is then calculated from the rates of fourfold simultaneous detections observed for a specific set of local projections.

one other particle. Thus, ES allows the establishment of entanglement between particles that have never interacted directly. By properly positioning the entanglement sources (EPR) and measurement devices across the communication channel, one can distribute entanglement without physically sending the individual quantum-correlated information carriers through the entire channel [see Figure 5.1(a)]. The ES is also applied in device-independent quantum communications or entanglement-assisted error correction [61, 62].

In previous demonstrations of ES, quantum repeaters, and relays, the authors used various methods to demonstrate successful operation of their schemes. For instance, Li *et al.* [130] used quantum-state tomography, Pan *et al.* [26] and de Riedmatten *et al.* [55] observed interference visibility and Jennewein *et al.* [131], Zhao *et al.* [132], and Yuan *et al.* [133] tested Bell inequality on the resulting state. This chapter discuses a practical method for diagnostics of ES by means of a collective entanglement witness (CEW) [91, 97–99]. We make use of the fact that the geometry of ES shares the layout of CEW (see Figure 5.1), both protocols require simultaneous preparation of two copies of a given potentially entangled state and a Bell-state projection. In particular, we adopt the collectibility witness originally proposed by Rudnicki et al. [56, 57]. This approach is preferable to diagnostics by other means as the method requires only six measurement config-

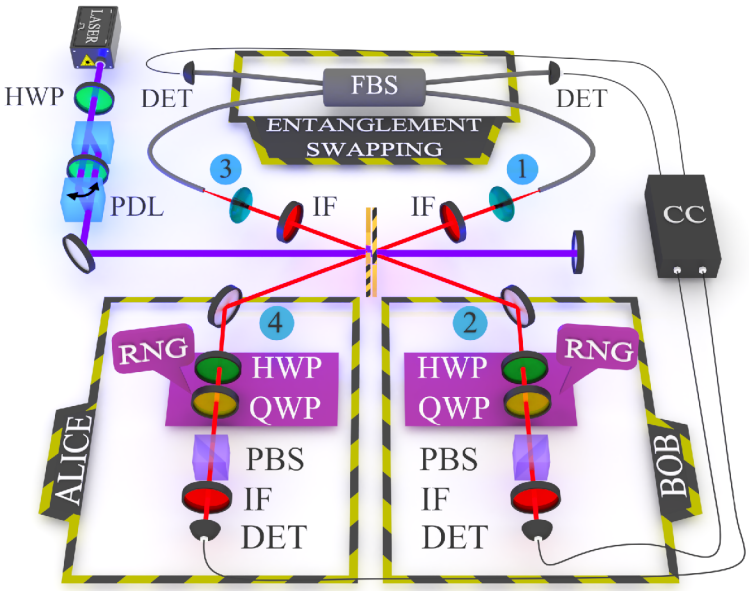

Figure 5.2: Experimental setup for diagnostics of the ES protocol. HWP: half-wave plate; QWP: quarter-wave plate; PBS: polarization beam splitter; PDL: polarization dispersion line; IF: interference filters; FBS: fiber beam splitter; DET: single-photon detector; CC: coincidence counter.

urations to calculate collectibility of a two-qubit state. A number that is smaller especially when compared to complete quantum state tomography [93, 94, 119]).

5.2 Experimental implementation

This idea is experimentally demonstrated on a linear-optical platform, where two independent EPR-state sources are constructed with an ES device linking them together. Qubits are encoded into polarization states of individual photons. Polarizers and wave plates are used to implement errors occurring in three distinct quantum-information channels, i.e., (a) a depolarizing channel, (b) a phase-damping channel, and (c) an amplitude-damping channel. In this experiment, both EPR pairs are subjected to the identically prepared damping channels (see Figure 5.2).

A frequency-doubled 413 nm femtosecond pulsed-laser beam is used to pump spontaneous parametric down-conversion in a β-BaB_2O_4 (BBO) crystal cascade [73]. At first, the pump polarization is made diagonal. Next, the beam travels through a polarization dispersion line (PDL) to counter subsequent polarization dispersion of the BBO material. This laser beam impinges on the crystal cascade twice, i.e., after it passes the crystals for the first time, it gets reflected on a mirror and pumps the crystals in the opposite direction. On both occasions, with

some probability, a pair of photons in the Bell state $|\Phi^+\rangle = \frac{1}{\sqrt{2}}(|HH\rangle + |VV\rangle)$ is generated, where H and V denote horizontally and vertically polarized photons, respectively. Using mirrors, pairs of photons generated by both the forward and backward propagating pumping beam are directed towards fiber couplers that lead them to single-photon detectors via single-mode optical fibers. These couplers are equipped with 10 nm interference filters in the case of photons 1 and 3 and by 5 nm interference filters in the case of photons 2 and 4. Typical four-photon detection event occurs about once per 4 min depending on the adjusted quantum state and polarization projection. The coincidences are accumulated for 10 h to collect about 150 events. The errors are calculated assuming Poisson statistics of the counts and using the Monte Carlo simulation. While polarization of photons 2 and 4 is projected locally on four states selected using combinations of half- and quarter-wave plates followed by polarizers, the other two photons (1 and 3) are projected onto a singlet state by means of a balanced fiber coupler (FBS) and postselected onto coincident detection at both its output ports.

The four specific settings of local projections sufficient to estimate collectibility [57] are $|HH\rangle$, $|HV\rangle$, $|VV\rangle$ and $|++\rangle$, where letters indicate state projections on the two locally projected photons, respectively, and $|+\rangle = \frac{1}{\sqrt{2}}(|H\rangle + |V\rangle)$. We denote p_{XY} ($\mathrm{XY} \in \{\mathrm{HH}, \mathrm{HV}, \mathrm{VV}, ++\}$) the probability that both locally projected photons pass the projections conditioned on the other two photons being projected onto a singlet Bell state. However, due to non-removable jitter between generation of the first and the second pair of photons, probability of two-photon overlap is decreased. Note that this jitter originates from the uncertainty in the moment in time when a pair is generated as the pumping pulse traverses the BBO crystal. It affects only interference of photons from two different pairs (forward and backward generated photon pairs) and is proportional to the length of the pumping pulse. Its effect on the observed interference visibility scales inversely with the coherence length of the generated photons, which can be extended by spectral filtering at the expense of losses [134, 135]. The imperfect temporal overlap between the photons caused by the aforementioned jitter is seen as noise, which can be estimated and subtracted from the genuine coincidences. In order to estimate the noise level both photon 1 and photon 3 are prepared in the same polarization state ($|H\rangle$) and the achievable Hong-Ou-Mandel (HOM) bunching effect is measured conditioned on detection of photon 2 and 4 (used as heralds). The observed HOM dip depth in this configuration is 43 % (perfect interference would result in 100 % dip depth). To compensate for the non-interacting photons, all projections are measured in two regimes: (a) adjusted for overlap between photons 1 and 3 and (b) with a completely detuned overlap so that the photons can not interfere. We then subtract 57 % of the coincidence counts obtained in both regimes and calculate the corrected HOM dip depth as their ratio. A more detailed account on this procedure is described in Ref. [58]. Measuring the

probabilities p_{XY}, collectibility is calculated using formula

$$\begin{aligned} W(\hat{\rho}) =& \tfrac{1}{2}[\eta + p_{\mathrm{H}}^2(1-2p_{\mathrm{HH}}) + (1-p_{\mathrm{H}})^2(1-2p_{\mathrm{VV}}) \\ &+ 2p_{\mathrm{H}}(1-p_{\mathrm{H}})(1-2p_{\mathrm{HV}}) - 1], \end{aligned} \tag{5.1}$$

where $\eta = 16p_{\mathrm{H}}(1-p_{\mathrm{H}})\sqrt{p_{\mathrm{HH}}p_{\mathrm{VV}}} + 4p_{++}$, and p_{H} is the probability of local projection of photon 1 or 3 onto horizontal polarization $|H\rangle$ independently of the singlet Bell-state projection.

For each measurement of the p_{XY} probabilities there was 16 setup configurations of wave plates for photons 2 and 4. It should be emphasized that six local projections at most are required to estimate collectibility. The 16 configurations mentioned above are needed to measure all these six collectibility projections for all state transformations required to implement the noisy channels described below. For example, projection onto a $|++\rangle$ state on photons 2 and 4 together with a phase flip transformation imposed to both these photons effectively requires measuring them in a $|--\rangle$ state ($|-\rangle = 1/\sqrt{2}(|H\rangle - |V\rangle)$). However, one should clearly distinguish the projections needed to measure collectibility from the state transformations imposed to deliberately implement various noisy channels. The latter would obviously not be performed when diagnosing a given entanglement-swapping device. Wave plates used for local polarization projections are used simultaneously to introduce disturbances typical for a given type of noisy quantum channel. As a result 16×60 sequences of fourfold coincidences are obtained. Depending on the simulated quantum channel a sequence is randomly with some bias selected and placed into a new array cc_{XY}, which in the end contained 60 randomly chosen sequences. The bias is dependent on the type of noisy quantum channel and on the chance for error to occur. The probability p_{XY} is then calculated by summation of cc_{XY}, normalization and correction on non-interacting photons. For the scheme of the experimental process see Figure 5.3.

Here, we experimentally investigate noisy channels studied theoretically in the context of quantum teleportation in Ref. [136]. In this experimental demonstration, we assume that noisy channels acting on both photons 2 and 4 are symmetric. In principle, these photons might be subject to different sources and amounts of noise. Our numerical analysis indicates that this effect would not generate any qualitatively new results. For the purposes of this proof-of-principle experiment, we are therefore limited to symmetric noisy channels.

We acquire the theoretical predictions for the below-described noisy channels by mathematical simulation of the collectibility measurement, where the initial Bell state $|\Phi^+\rangle$ is subjected to Kraus operators for various damping values obtaining the transformed state $\hat{\rho}$. Two copies of the transformed state are used to

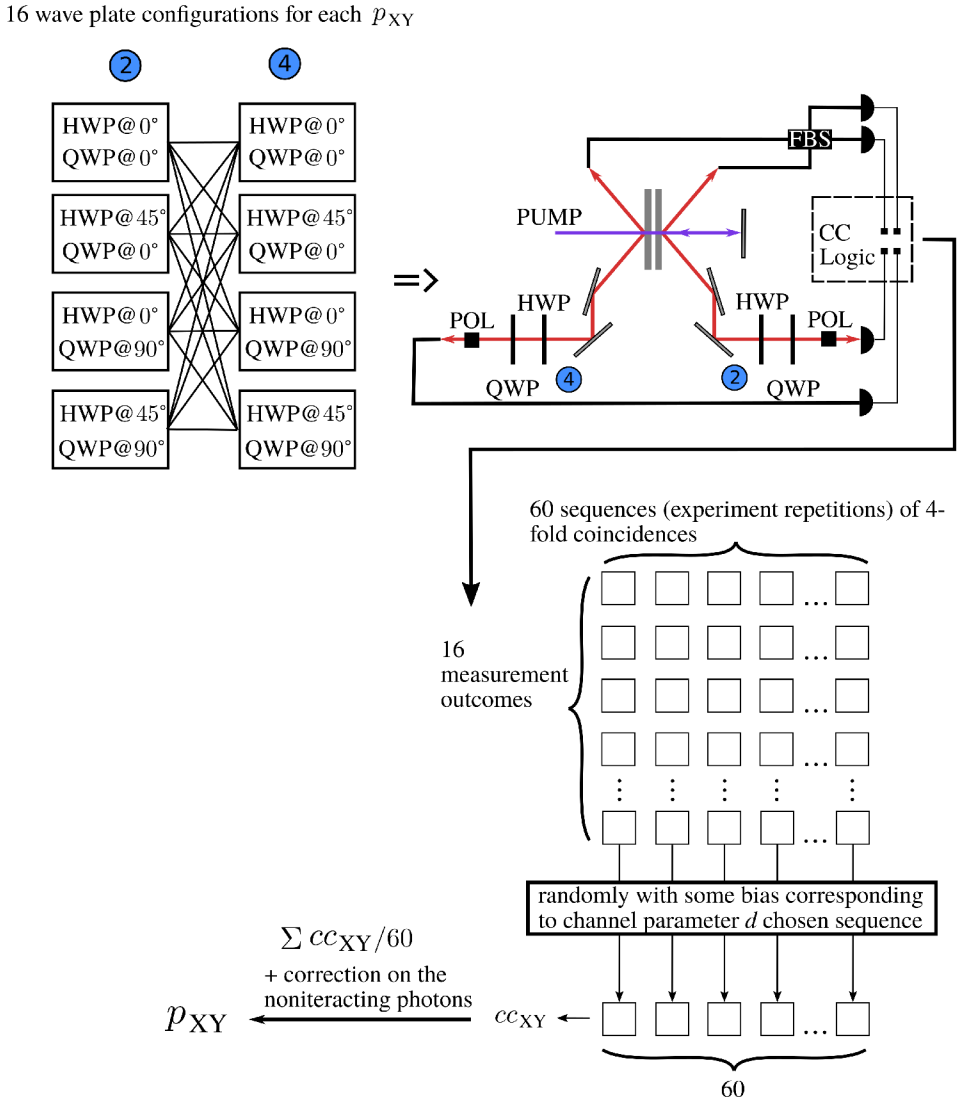

Figure 5.3: Scheme of the experimental process of simulating noisy quantum channels.

calculate the probabilities p_{H}, p_{XY}

$$p_{\mathrm{H}} = \mathrm{Tr}[|H\rangle\langle H|\hat{\mathbb{1}}_2\ \hat{\rho}], \tag{5.2}$$

$$p_{\mathrm{XY}} = \frac{\mathrm{Tr}[|X\rangle\langle X|\Psi^-\rangle\langle\Psi^-|Y\rangle\langle Y|\ \hat{\rho}\otimes\hat{\rho}]}{\mathrm{Tr}[|X\rangle\langle X|\hat{\mathbb{1}}_4|Y\rangle\langle Y|\ \hat{\rho}\otimes\hat{\rho}]} \tag{5.3}$$

and subsequently the collectibility.

5.2.1 Depolarizing channel

Qubits transmitted through a depolarizing channel are randomly subjected to three types of transformations causing decoherence. These transformations are bit

flip, phase flip, and a combination of bit flip and phase flip. It is the randomness and impossibility to predict these transformations that is the effective cause of errors. The action of a depolarizing channel expressed by Kraus operators [21] reads

$$\hat{E}_0 = \sqrt{1-d_{\mathrm{D}}}\hat{I},\ \hat{E}_i = \sqrt{\frac{d_{\mathrm{D}}}{3}}\hat{\sigma}_i \quad \text{for } i \in \{x,y,z\}, \tag{5.4}$$

where d_{D} is the depolarization probability, $\hat{I}$ stands for the identity operator and σ_i are Pauli matrices. When propagating through such channel, a Bell state is randomly transformed into one of the other three Bell states with equal probability $d_{\mathrm{D}}/3$. The implementation of depolarizing channel, was realized by randomly switching half-wave plates and quarter-wave plates between two positions: 0° and 45° for the HWPs and 0° and 90° for the QWPs. Using the procedure described in the previous paragraph we are able to measure the collectibility of a Bell state propagating through depolarizing channel for several values of the depolarization probability d_{D}. The observed collectibility and its theoretical prediction are depicted in Figure 5.4(a). As expected, collectibility reaches its maximum value for $d_{\mathrm{D}} = 3/4$, $W(\hat{\rho}) = 0.80 \pm 0.09$ (theoretical prediction: $W(\hat{\rho}) = 0.75$). This corresponds to a maximally depolarizing action causing the transmitted state to fully decohere to $\hat{\rho}_{\mathrm{D}} = \hat{\mathbb{1}}/4$. Meanwhile, in an ideal channel ($d_{\mathrm{D}} = 0$) the Bell state is propagating undisturbed which coincides with the value of collectibility being $W(\hat{\rho}) = -0.24 \pm 0.06$ (theoretical prediction: $W(\hat{\rho}) = -0.25$).

5.2.2 Phase-damping channel

The effect of phase damping causes decoherence between two basis qubit states without, however, causing any bit flip transformation. Such channel can be described by two Kraus operators

$$\hat{E}_0 = \sqrt{1-\frac{d_{\mathrm{P}}}{2}}\hat{I}, \qquad \hat{E}_1 = \sqrt{\frac{d_{\mathrm{P}}}{2}}\hat{\sigma}_z, \tag{5.5}$$

where d_{P} is the dephasing probability. Similarly to the previous case, the phase-damping effect was implemented by randomly switching quarter-wave plates between two positions: 0° and 90°. The resulting collectibility as a function of d_{P} is presented in Figure 5.4(b). Experimental value of collectibility at $d_{\mathrm{P}} = 1$ reaches $W(\hat{\rho}) = 0.32 \pm 0.09$ (theoretical prediction: $W(\hat{\rho}) = 0.25$) as the Bell state propagating through this channel becomes $\hat{\rho}_{\mathrm{P}} = \frac{1}{2}(|HH\rangle\langle HH| + |VV\rangle\langle VV|)$.

5.2.3 Amplitude-damping channel

Typically, amplitude damping causes lossy transmission of qubits through the channel. The overall losses are trivial to detect as they decrease the overall number of coincident detections. Apart from that, white (state-independent) losses do not

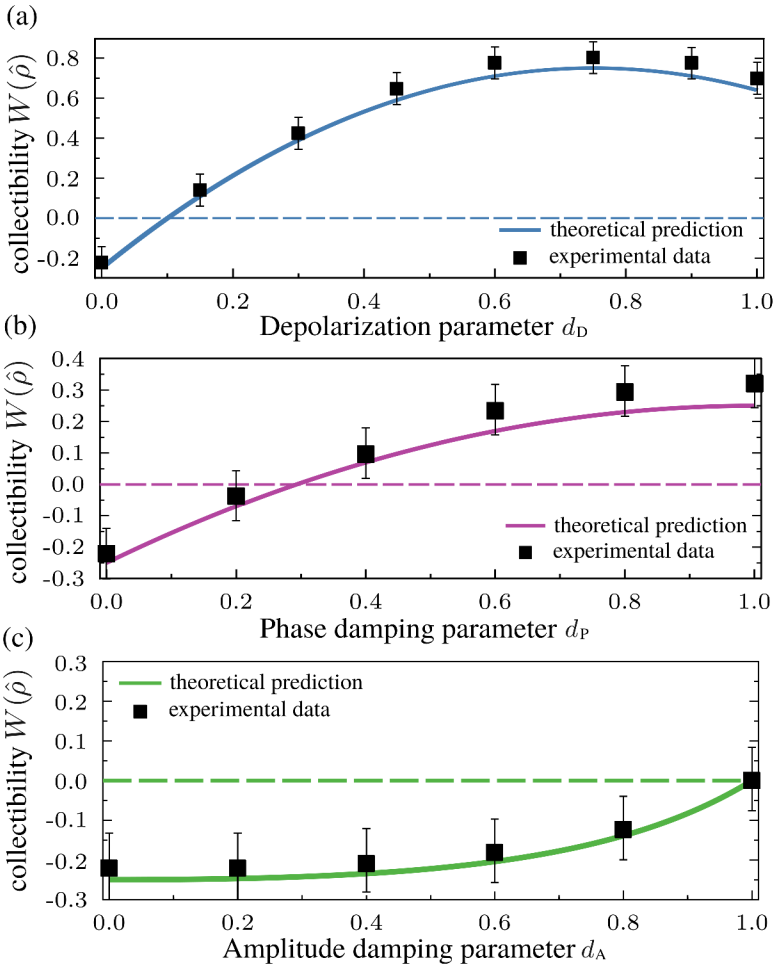

Figure 5.4: Measured collectibility after the EPR pairs pass through: (a) depolarizing channel (b) phase-damping channel (c) amplitude-damping channel parameterized by parameter d_D, d_P and d_A respectively.

change the collectibility because the measurement relies solely on successful four-photon detections. It is, therefore, more interesting to analyse state-dependent (polarization sensitive) losses that cause disturbance in superposition of horizontal and vertical polarizations of the state. One can describe this channel by an effective matrix transformation

$$\hat{\rho} \to \hat{E}_A \hat{\rho} \hat{E}_A^\dagger, \qquad \hat{E}_A = \begin{pmatrix} 1 & 0 \\ 0 & \sqrt{1-d_A} \end{pmatrix}. \tag{5.6}$$

Here, in contrast to the above-described channels, the entangled state remains pure but its entanglement decreases. This corresponds to the Bell state being less entangled $\frac{1}{\sqrt{2-d_A}}(|HH\rangle + (1-d_A)|VV\rangle)$ and eventually becoming separable $\hat{\rho}_A = |HH\rangle\langle HH|$ as $d_A \to 1$, where the value of collectibility reaches $W(\hat{\rho}) = -0.05 \pm 0.09$ (theoretical prediction: $W(\hat{\rho}) = 0$). Collectibility allows this transition to be

captured as shown in Figure 5.4(c). Note that the CEW for pure states can serve as an entanglement measure [56, 57].

To simulate the effect of amplitude damping on the p_{H} probability the fourfold coincidences outside of the HOM dip (without Bell-state measurement) were measured while projecting photons 2 and 4 onto HH and VV polarizations. Note that p_{HH} /p_{VV} probability outside of dip is equal to p_{H}^2 /$(1-p_{\mathrm{H}})^2$. Both projections consisted of 74 measurements each taking 10 min. Given the four-photon detection rate and length of the time, the number of coincidences detected in each of the 74 sequences fluctuated from 0 to about 5. The 74 sequences of coincidences were then organized in a decreasing and increasing order for the HH and VV polarizations, respectively. The ratio R was introduced as

$$\frac{\sum_{n=1}^{N} cc_{\mathrm{HH}}(n)}{\sum_{n=1}^{N} cc_{\mathrm{VV}}(n)} = R(N) = \frac{p_{\mathrm{H}}^2}{(1-p_{\mathrm{H}})^2}, \quad N \in [1, 74] \tag{5.7}$$

from which the probability p_{H} was obtained by solving the quadratic equation Eq. (5.7).

5.2.4 Channel characteristics

Measurement of collectibility is a powerful tool that allows detection of disturbance occurring in the channel. However, in order to promote this method even further, analysis of characteristic effects of the three types of noisy channels was performed. By detailed analysis of the individual probabilities used for collectibility calculation one can identify which type of damping is inflicted. Five probabilities are measured to calculate collectibility p_{XY} for $\mathrm{XY} \in \{\mathrm{HH}, \mathrm{HV}, \mathrm{VV}, {+}{+}\}$, and p_{H}. The experimental and theoretical values of these quantities for three tested channels and a reference perfect channel are visualized in Figure 5.5. The exact results are then summarized in Table 5.1. For a perfect channel the overall state of the system is

$$|\Phi^+\rangle|\Phi^+\rangle = \tfrac{1}{2}[(|HH\rangle + |VV\rangle)(|HH\rangle + |VV\rangle)], \tag{5.8}$$

which after projecting the photons 1 and 3 onto a singlet state collapses also to a singlet state

$$|\Phi^+\rangle|\Phi^+\rangle \xrightarrow{|\psi_{13}^-\rangle\langle\psi_{13}^-|} |\psi_{24}^-\rangle. \tag{5.9}$$

Hence, the only conditioned projection that one observes is the $|HV\rangle$ projection with probability p_{HV} of 1/2. It follows from the Eq. (5.8) that the probability p_{H} of unconditional projection $|H\rangle$ is also 1/2. In a fully depolarizing channel the state of the system becomes maximally mixed

$$\hat{\rho}_{\mathrm{D}} \otimes \hat{\rho}_{\mathrm{D}} = \hat{\mathbb{1}}/16 \xrightarrow{|\psi_{13}^-\rangle\langle\psi_{13}^-|} \hat{\mathbb{1}}_{24}/4. \tag{5.10}$$

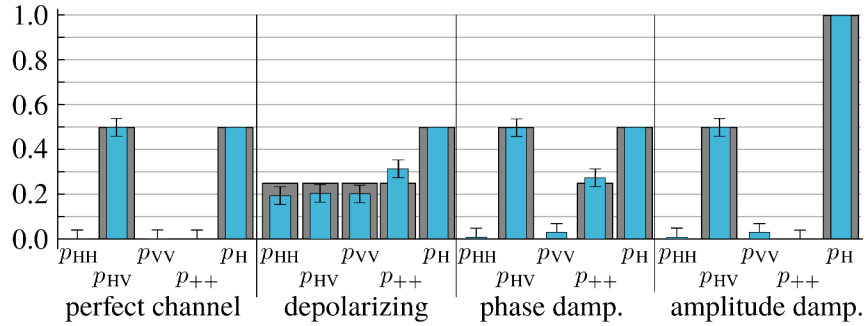

Figure 5.5: Characteristic channel signatures allowing to identify type of errors from the individual measurements that constitute collectibility. Gray and blue bars represent theoretical predictions and experimentally obtained values respectively. The uncertainty of the unconditioned probability p_H is negligible, therefore, is not visualized.

Therefore, all of the conditional projections are equally likely with probabilities of 1/4. The probability p_H of unconditional projection $|H\rangle$ stays at 1/2. Phase damping transforms the initial Bell state into a $\hat{\rho}_P$. The final state of the photons 2 and 4 is then

$$\hat{\rho}_P \otimes \hat{\rho}_P \xrightarrow{|\psi_{13}^-\rangle\langle\psi_{13}^-|} \tfrac{1}{2}(|H_2V_4\rangle\langle H_2V_4| + |V_2H_4\rangle\langle V_2H_4|). \tag{5.11}$$

The probability of observing a conditional $|HV\rangle$ projection is 1/2, however, due to the phase flip transformation we also observe signal in $|++\rangle$ projection with probability p_{++} of 1/4. The unconditional projection $|H\rangle$ happens with probability 1/2. In an amplitude-damping channel with attenuated vertical polarization, the not normalized state of the photons 2 and 4 becomes

$$|\Phi^+\rangle|\Phi^+\rangle \xrightarrow{|\psi_{13}^-\rangle\langle\psi_{13}^-|} \frac{1}{2\sqrt{2}}\sqrt{1-d_A}\big(|H_2\rangle|V_4\rangle - |V_2\rangle|H_4\rangle\big). \tag{5.12}$$

Post-selection of photons 1 and 3 onto a singlet Bell state, steers the state of photons 2 and 4 onto a perfect Bell state independently of the amplitude damping parameter d_A hence the probabilities p_{XY} remain unchanged. On the other hand, the d_A parameter affects the probability of successful post-selection of photons 1 and 3 onto a singlet state as well as the local probability p_H. In case of a completely damping channels $d_A = 1$, p_H becomes 1 and the collectibility W becomes 0 as correctly expected for a separable state of photons 1 and 2 and 3 and 4 respectively.

5.2.5 Imperfect Bell-state measurement

To explicitly demonstrate that imperfect Bell-state projection also has a measurable effect and can be detected, we calculated the probabilities p_{XY} without the

Table 5.1: Experimental results and theoretical prediction (in parenthesis) of the p_{XY} and p_{H} probabilities and collectibility obtained for the perfect, fully depolarizing, fully phase-damping and fully amplitude-damping channel. The uncertainty of conditional probabilities p_{XY} and unconditional probability p_{H} is 4% and less than 1% respectively. The uncertainty of collectibility measurement is ± 0.09.

	perfect channel	depolarizing channel	phase-dam. channel	amplitude-dam. channel
$p_{\mathrm{HH}}(\%)$	1 (0)	20 (25)	1 (0)	1 (0)
$p_{\mathrm{HV}}(\%)$	50 (50)	21 (25)	50 (50)	50 (50)
$p_{\mathrm{VV}}(\%)$	3 (0)	20 (25)	3 (0)	3 (0)
$p_{++}(\%)$	1 (0)	32 (25)	28 (25)	0 (0)
$p_{\mathrm{H}}(\%)$	50 (50)	50 (50)	50 (50)	100 (100)
$W(\hat{\rho})$	-0.22 (-0.25)	0.81 (0.75)	0.33 (0.25)	-0.01 (0.00)

compensation for non-interacting photons. This is specific to the linear-optical platform, where Bell-state projection is implemented by two-photon interference. The obtained values are $p_{\mathrm{HH}} = 0.29$, $p_{\mathrm{HV}} = 0.49$, $p_{\mathrm{VV}} = 0.27$ and $p_{++} = 0.29$, with typical uncertainty of 0.03. The resulting collectibility reads $W = 0.75 \pm 0.06$. These results prove that imperfect Bell-state projection by a balanced beam splitter is also detected by our method and additionally manifests a unique signature: the probability p_{HV} should maintain a value of 0.5 as in the case of a perfect channel, whereas the remaining probabilities should uniformly increase their values from 0 (perfect Bell-state projection) up to 0.5 (Bell-state projection replaced by completely non-interfering photons). Consequently, the imperfections in Bell-state projection can be distinguished from the channel imperfections. Our experimental results reflect the fact that the Bell-state measurement is imperfect only to some degree. The portion of non-interacting photons in the Hong-Ou-Mandel cross-pair interference is 57 %.

5.3 Conclusions

This work reports on the experimental diagnostics of entanglement swapping by utilizing four partial measurements applied for determining CEW (collectibility). With this approach one can capitalize on the similarity between the geometry of the ES protocol and the layout for measurement of CEW. This method allows detection of disturbance in a channel by measuring four probabilities p_{XY} and estimating the collectibility making it a preferable method as the number of measurement configurations is lower than in other means of diagnostics. The

collectibility was measured for three noisy channels: depolarizing channel, phase-damping channel, and amplitude-damping channel. The obtained experimental data is in a good agreement with theoretical predictions. Additionally, by analysis of the measured p_{XY} probabilities, one can determine which type of error is occurring in a given experimental setting for all three damping channels. The experiment also demonstrate that this approach is able to detect imperfections in Bell-state measurement and is capable of distinguishing them from previously mentioned faulty channels. A real-world channel may constitute a combination of typical noisy channels (depolarizing, dephasing) and hence the observed channel characteristics reflected in the measured probabilities p_{XY} would be a combination of characteristics of the participating types of noise. This effect, however, does not change qualitatively any of the presented results and drawn conclusions. We believe that these results can contribute to the field of quantum communications and mainly represent a practical instrument for future deployment of quantum networks or engineering of complex multilevel quantum systems.

Chapter 6

Conclusions

As described in the introduction, quantum information processing realized on the platform of linear optics represents a perspective area of research. In recent years it accomplished several milestones such as controlled and long-distance quantum teleportation or secure quantum key distribution. Nevertheless, there are still many concepts that need to be theoretically investigated and experimentally demonstrated.

In this thesis, three original QIP experiments were presented. They were motivated by recent developments in the field and by our believe that they might contribute to the advancement of quantum information processing. The focuses of these experiments were the detection of entanglement in hyper-entangled states, characterization of errors that could occur during an entanglement swapping and a distance measure between quantum states. To our satisfaction, all of our results were published in journals with an impact factor. In one case the results were deemed important enough to warrant publication in the prestigious Physical Review Letters. These results were also promoted to general public via several media [137–139].

The first experiment, presented in Chapter 3, successfully demonstrated the detection of entanglement in a hyper-entangled state by a non-linear entanglement witness. The original technique which was proposed by Rudnicki *et al.* allows to detect entanglement in large number of two-qubit states. The collectibility measurement of systems entangled in one degree of freedom requires to perform the collective measurements on two identical copies of the investigated state. Here the collectibility was measured directly on a single multilevel state where a two-qubit state is copied across two degrees of freedom. Advantage of the mixed encoding is that one needs fewer information carriers (photons) therefore, the detection events are more frequent and the whole measurement is considerably faster. Further to that, complete Bell analysis is feasible with linear optics when two degrees of freedom are involved.

The fourth Chapter presents the second experiment which was focused on

the measurement of Hilbert-Schmidt distance between two two-qubit states. The experiment demonstrates that our method for measuring Hilbert-Schmidt distance is far less complex than reconstructing density matrices and that it can be applied in quantum-enhanced machine learning to reduce the complexity of calculating Euclidean distances between multidimensional points. The results are also a novel example of applying mixed states in quantum information processing. Usually working with mixed states is undesired, but here it gives the possibility of encoding extra information as coherence between given two dimensions of the density matrix.

The third experiment is discussed in Chapter 5. It aimed at the diagnostics of entanglement swapping protocol by means of collectibility. The experiment successfully demonstrated that our approach is suitable to detect disturbances occurring in the preparation of quantum states, quantum communication channel and imperfect Bell-state projection. Advantage of this method is that there is considerable similarity between the geometry of the entanglement swapping protocol and the layout for collectibility measurement.

In addition to the three experiments described in this thesis, the author is also a co-author of other two publications. One is related to the distance measures in Hilbert space [A2], the other to the characterization of photon-number noise in Rarity-Tapster-Loudon-type interferometers [A5] published as a summary of authors Master's thesis. The first paper is a theoretical study into direct measurement of quantum state distances investigated during the author's research visit to prof. Karol Bartkiewicz at Adam Mickiewicz University in Poland.

There are still many compelling topics and concepts whether related or unrelated to the discussed experiments that deserve some attention. The author believes that he might pursue some of them in his future work.

Author's publications

[A1] V. Trávníček, K. Bartkiewicz, A. Černoch, and K. Lemr, "Experimental measurement of the hilbert-schmidt distance between two-qubit states as a means for reducing the complexity of machine learning", Phys. Rev. Lett. **123**, 260501 (2019).

[A2] K. Bartkiewicz, V. Trávníček, and K. Lemr, "Measuring distances in hilbert space by many-particle interference", Phys. Rev. A **99**, 032336 (2019).

[A3] V. Trávníček, K. Bartkiewicz, A. Černoch, and K. Lemr, "Experimental measurement of a nonlinear entanglement witness by hyperentangling two-qubit states", Phys. Rev. A **98**, 032307 (2018).

[A4] V. Trávníček, K. Bartkiewicz, A. Černoch, and K. Lemr, "Experimental diagnostics of entanglement swapping by a collective entanglement test", Phys. Rev. Applied **14**, 064071 (2020).

[A5] V. Trávníček, K. Bartkiewicz, A. Černoch, and K. Lemr, "Experimental characterization of photon-number noise in rarity-tapster-loudon-type interferometers", Phys. Rev. A **96**, 023847 (2017).

References

[1] M. O. Scully and M. S. Zubairy, *Quantum optics* (Cambridge University Press, 1997).

[2] G. S. Agarwal, *Quantum optics* (Cambridge University Press, 2012).

[3] P. Meystre and M. Sargent, *Elements of quantum optics* (Springer-Verlag Berlin Heidelberg, 2007).

[4] U. L. Andersen, T. Gehring, C. Marquardt, and G. Leuchs, "30 years of squeezed light generation", Physica Scripta **91**, 053001 (2016).

[5] F. J. Mcclung and R. W. Hellwarth, "Giant optical pulsations from ruby", Journal of Applied Physics **33**, 828–829 (1962).

[6] L. E. Hargrove, R. L. Fork, and M. A. Pollack, "Locking of he–ne laser modes induced by synchronous intracavity modulation", Applied Physics Letters **5**, 4–5 (1964).

[7] A. M. Weiner, *Ultrafast optics* (Wiley, 2009).

[8] A. Ashkin, J. M. Dziedzic, J. E. Bjorkholm, and S. Chu, "Observation of a single-beam gradient force optical trap for dielectric particles", Optics Letters **11**, 288 (1986).

[9] T. Hänsch and A. Schawlow, "Cooling of gases by laser radiation", Optics Communications **13**, 68–69 (1975).

[10] J. Dalibard and C. Cohen-Tannoudji, "Laser cooling below the doppler limit by polarization gradients: simple theoretical models", Journal of the Optical Society of America B **6**, 2023 (1989).

[11] S. J. Freedman and J. F. Clauser, "Experimental test of local hidden-variable theories", Phys. Rev. Lett. **28**, 938–941 (1972).

[12] A. Aspect, P. Grangier, and G. Roger, "Experimental realization of einstein-podolsky-rosen-bohm gedankenexperiment: a new violation of bell's inequalities", Phys. Rev. Lett. **49**, 91–94 (1982).

[13] D. Boschi, S. Branca, F. De Martini, L. Hardy, and S. Popescu, "Experimental realization of teleporting an unknown pure quantum state via dual classical and einstein-podolsky-rosen channels", Phys. Rev. Lett. **80**, 1121–1125 (1998).

[14] D. Bouwmeester, J.-W. Pan, K. Mattle, M. Eibl, H. Weinfurter, and A. Zeilinger, "Experimental quantum teleportation", Nature **390**, 575–579 (1997).

[15] A. Barenco, C. H. Bennett, R. Cleve, D. P. DiVincenzo, N. Margolus, P. Shor, T. Sleator, J. A. Smolin, and H. Weinfurter, "Elementary gates for quantum computation", Phys. Rev. A **52**, 3457–3467 (1995).

[16] L. K. Grover, "Quantum mechanics helps in searching for a needle in a haystack", Phys. Rev. Lett. **79**, 325–328 (1997).

[17] P. W. Shor, "Polynomial-time algorithms for prime factorization and discrete logarithms on a quantum computer", SIAM Journal on Computing **26**, 1484–1509 (1997).

[18] W. K. Wootters and W. H. Zurek, "A single quantum cannot be cloned", Nature **299**, 802–803 (1982).

[19] C. H. Bennett and G. Brassard, "Quantum cryptography: public key distribution and coin tossing", Theoretical Computer Science **560**, 7–11 (2014).

[20] A. K. Ekert, "Quantum cryptography based on bell's theorem", Phys. Rev. Lett. **67**, 661–663 (1991).

[21] M. A. Nielsen and I. L. Chuang, *Quantum computation and quantum information* (Cambridge University Press, 2010).

[22] B. Schumacher, "Quantum coding", Phys. Rev. A **51**, 2738–2747 (1995).

[23] C.-Y. Lu, D. E. Browne, T. Yang, and J.-W. Pan, "Demonstration of a compiled version of shor's quantum factoring algorithm using photonic qubits", Phys. Rev. Lett. **99**, 250504 (2007).

[24] E. Lucero, R. Barends, Y. Chen, J. Kelly, M. Mariantoni, A. Megrant, P. O'Malley, D. Sank, A. Vainsencher, J. Wenner, and et al., "Computing prime factors with a josephson phase qubit quantum processor", Nature Physics **8**, 719–723 (2012).

[25] H.-J. Briegel, W. Dür, J. I. Cirac, and P. Zoller, "Quantum repeaters: the role of imperfect local operations in quantum communication", Phys. Rev. Lett. **81**, 5932–5935 (1998).

[26] J.-W. Pan, D. Bouwmeester, H. Weinfurter, and A. Zeilinger, "Experimental entanglement swapping: entangling photons that never interacted", Phys. Rev. Lett. **80**, 3891–3894 (1998).

[27] B. C. Jacobs, T. B. Pittman, and J. D. Franson, "Quantum relays and noise suppression using linear optics", Phys. Rev. A **66**, 052307 (2002).

[28] P. Rabl, D. DeMille, J. M. Doyle, M. D. Lukin, R. J. Schoelkopf, and P. Zoller, "Hybrid quantum processors: molecular ensembles as quantum memory for solid state circuits", Phys. Rev. Lett. **97**, 033003 (2006).

[29] A. I. Lvovsky, B. C. Sanders, and W. Tittel, "Optical quantum memory", Nature Photonics **3**, 706–714 (2009).

[30] C. H. Bennett, H. J. Bernstein, S. Popescu, and B. Schumacher, "Concentrating partial entanglement by local operations", Phys. Rev. A **53**, 2046–2052 (1996).

[31] C. H. Bennett, G. Brassard, S. Popescu, B. Schumacher, J. A. Smolin, and W. K. Wootters, "Purification of noisy entanglement and faithful teleportation via noisy channels", Phys. Rev. Lett. **76**, 722–725 (1996).

[32] D. Wineland, M. Barrett, J. Chiaverini, B. DeMarco, W. Itano, B. Jelenkovic, C. Langer, D. Leibfried, V. Meyer, T. Rosenband, and T. Schätz, "Quantum information processing with trapped ions", Philosophical transactions. Series A, Mathematical, physical, and engineering sciences **361**, 1349–61 (2003).

[33] L. Vandersypen, M. Steffen, G. Breyta, C. Yannoni, M. Sherwood, and I. Chuang, "Experimental realization of shor's quantum factoring algorithm using nuclear magnetic resonance.", Nature **414**, 883–7 (2001).

[34] A. Blais, S. M. Girvin, and W. D. Oliver, "Quantum information processing and quantum optics with circuit quantum electrodynamics", Nature Physics **16**, 247–256 (2020).

[35] M. Krenn, M. Malik, T. Scheidl, R. Ursin, and A. Zeilinger, "Quantum communication with photons", Optics in Our Time, 455–482 (2016).

[36] G. Jaeger, *Quantum information: an overview* (Springer, 2010).

[37] A. Barasiński, A. Černoch, and K. Lemr, "Demonstration of controlled quantum teleportation for discrete variables on linear optical devices", Phys. Rev. Lett. **122**, 170501 (2019).

[38] C. Croal, C. Peuntinger, B. Heim, I. Khan, C. Marquardt, G. Leuchs, P. Wallden, E. Andersson, and N. Korolkova, "Free-space quantum signatures using heterodyne measurements", Phys. Rev. Lett. **117**, 100503 (2016).

[39] T. M. Mitchell, *Machine learning* (MacGraw-Hill, 1997).

[40] P. Wittek, *Quantum machine learning: what quantum computing means to data mining* (Elsevier, 2014).

[41] M. P. Deisenroth, A. A. Faisal, and C. S. Ong, *Mathematics for machine learning* (Cambridge University Press, 2020).

[42] J. Biamonte, P. Wittek, N. Pancotti, P. Rebentrost, N. Wiebe, and S. Lloyd, "Quantum machine learning", Nature **549**, 195–202 (2017).

[43] W. A. J. Kosmala, *A friendly introduction to analysis: single and multivariable* (Pearson Education Taiwan Ltd., 2009).

[44] S. Lloyd, M. Mohseni, and P. Rebentrost, *Quantum algorithms for supervised and unsupervised machine learning*, 2013.

[45] S. Lloyd, M. Mohseni, and P. Rebentrost, "Quantum principal component analysis", Nature Physics **10**, 631–633 (2014).

[46] P. Rebentrost, M. Mohseni, and S. Lloyd, "Quantum support vector machine for big data classification", Physical Review Letters **113** (2014).

[47] N. Wiebe, A. Kapoor, and K. M. Svore, "Quantum algorithms for nearest-neighbor methods for supervised and unsupervised learning", Quantum Inf. Comput. **15**, 316–356 (2015).

[48] A. Choromanska, M. Henaff, M. Mathieu, G. B. Arous, and Y. LeCun, *The loss surfaces of multilayer networks*, 2015.

[49] N. Datta, C. Hirche, and A. Winter, "Convexity and operational interpretation of the quantum information bottleneck function", 2019 IEEE International Symposium on Information Theory (ISIT) (2019).

[50] A. Černoch, "Experimentální přenos a zpracování kvantové informace v podobě polarizačního stavu fotonu", Ph.D. thesis, Palacký University Olomouc (2006).

[51] J. Soubusta, "Využití sestupné frekvenční parametrické konverze v optických experimentech", assoc. professor's thesis, Palacký University Olomouc (2009).

[52] K. Lemr, "Quantum information processing with the tunable controlled-phase gate", assoc. professor's thesis, Palacký University Olomouc (2016).

[53] F. Mintert, A. R. Carvalho, M. Kuś, and A. Buchleitner, "Measures and dynamics of entangled states", Physics Reports **415**, 207–259 (2005).

[54] R. Horodecki, P. Horodecki, M. Horodecki, and K. Horodecki, "Quantum entanglement", Rev. Mod. Phys. **81**, 865–942 (2009).

[55] H. de Riedmatten, I. Marcikic, W. Tittel, H. Zbinden, D. Collins, and N. Gisin, "Long distance quantum teleportation in a quantum relay configuration", Phys. Rev. Lett. **92**, 047904 (2004).

[56] Ł. Rudnicki, P. Horodecki, and K. Życzkowski, "Collective uncertainty entanglement test", Phys. Rev. Lett. **107**, 150502 (2011).

[57] Ł. Rudnicki, Z. Puchała, P. Horodecki, and K. Życzkowski, "Collectibility for mixed quantum states", Phys. Rev. A **86**, 062329 (2012).

[58] K. Lemr, K. Bartkiewicz, and A. Černoch, "Experimental measurement of collective nonlinear entanglement witness for two qubits", Phys. Rev. A **94**, 052334 (2016).

[59] I. Bengtsson and K. Życzkowski, *Geometry of quantum states: an introduction to quantum entanglement* (Cambridge University Press, 2017).

[60] J. Dajka, J. Łuczka, and P. Hänggi, "Distance between quantum states in the presence of initial qubit-environment correlations: a comparative study", Phys. Rev. A **84**, 032120 (2011).

[61] M. Curty and T. Moroder, "Heralded-qubit amplifiers for practical device-independent quantum key distribution", Phys. Rev. A **84**, 010304 (2011).

[62] T. Brun, I. Devetak, and M.-H. Hsieh, "Correcting quantum errors with entanglement", Science **314**, 436–439 (2006).

[63] R. B. Griffiths, *Consistent quantum theory* (Cambridge University Press, 2004).

[64] C. E. Shannon, "A mathematical theory of communication", The Bell System Technical Journal **27**, 379–423 (1948).

[65] J. Roik, K. Lemr, A. Černoch, and K. Bartkiewicz, "Interplay between strong and weak measurement: comparison of three experimental approaches to weak value estimation", Journal of Optics **22**, 065202 (2020).

[66] M. Mohseni, A. M. Steinberg, and J. A. Bergou, "Optical realization of optimal unambiguous discrimination for pure and mixed quantum states", Phys. Rev. Lett. **93**, 200403 (2004).

[67] I. Marcikic, H. de Riedmatten, W. Tittel, H. Zbinden, M. Legré, and N. Gisin, "Distribution of time-bin entangled qubits over 50 km of optical fiber", Phys. Rev. Lett. **93**, 180502 (2004).

[68] J. Heersink, C. Marquardt, R. Dong, R. Filip, S. Lorenz, G. Leuchs, and U. L. Andersen, "Distillation of squeezing from non-gaussian quantum states", Phys. Rev. Lett. **96**, 253601 (2006).

[69] S. L. Braunstein and P. van Loock, "Quantum information with continuous variables", Rev. Mod. Phys. **77**, 513–577 (2005).

[70] R. W. Boyd, *Nonlinear optics* (Elsevier, Acad. Press, 2011).

[71] S. Karan, S. Aarav, H. Bharadhwaj, L. Taneja, A. De, G. Kulkarni, N. Meher, and A. K. Jha, "Phase matching in beta-barium borate crystals for spontaneous parametric down-conversion", Journal of Optics **22**, 083501 (2020).

[72] A. Černoch, J. Soubusta, L. Bartůšková, M. Dušek, and J. Fiurášek, "Experimental implementation of partial symmetrization and anti-symmetrization of two-qubit states", New Journal of Physics **11**, 023005 (2009).

[73] P. G. Kwiat, E. Waks, A. G. White, I. Appelbaum, and P. H. Eberhard, "Ultrabright source of polarization-entangled photons", Phys. Rev. A **60**, R773–R776 (1999).

[74] B. E. A. Saleh and M. C. Teich, *Fundamentals of photonics* (Wiley-Interscience, 2009).

[75] L. N. Hadley and D. M. Dennison, "Reflection and transmission interference filters part i. theory", J. Opt. Soc. Am. **37**, 451–465 (1947).

[76] N. Ismail, C. C. Kores, D. Geskus, and M. Pollnau, "Fabry-Perot resonator: spectral line shapes, generic and related airy distributions, linewidths, finesses, and performance at low or frequency-dependent reflectivity", Opt. Express **24**, 16366–16389 (2016).

[77] H. A. Macleod, *Thin-film optical filters* (CRC Press, Taylor & Francis Group, 2018).

[78] A. Migdall, S. Polyakov, J. Fan, and J. Bienfang, *Single-photon generation and detection: physics and applications* (Academic Press, 2014).

[79] G. H. Rieke, *Detection of light: from the ultraviolet to the submillimeter* (Cambridge University Press, 2009).

[80] M. Ježek, J. Fiurášek, and Z. Hradil, "Quantum inference of states and processes", Phys. Rev. A **68**, 012305 (2003).

[81] A. Einstein, B. Podolsky, and N. Rosen, "Can quantum-mechanical description of physical reality be considered complete?", Physical Review **47**, 777–780 (1935).

[82] A. Einstein, M. Born, and H. Born, *The born-einstein letters; correspondence between albert einstein and max and hedwig born from 1916 to 1955* (Walker, 1971).

[83] E. Schödinger, "Discussion of probability relations between separated systems", Mathematical Proceedings of the Cambridge Philosophical Society **31**, 555–563 (1935).

[84] J. Bell, "On the einstein podolsky rosen paradox", Phsyics **1**, 195 (1964).

[85] J. F. Clauser, M. A. Horne, A. Shimony, and R. A. Holt, "Proposed experiment to test local hidden-variable theories", Phys. Rev. Lett. **23**, 880–884 (1969).

[86] N. Brunner, D. Cavalcanti, S. Pironio, V. Scarani, and S. Wehner, "Bell nonlocality", Rev. Mod. Phys. **86**, 419–478 (2014).

[87] O. Gühne and G. Töth, "Entanglement detection", Physics Reports **474**, 1–75 (2009).

[88] O. Gühne and N. Lütkenhaus, "Nonlinear entanglement witnesses", Phys. Rev. Lett. **96**, 170502 (2006).

[89] T. Moroder, O. Gühne, and N. Lütkenhause, "Iterations of nonlinear entanglement witnesses", Phys. Rev. A **78**, 032326 (2008).

[90] J. M. Arrazola, O. Gittsovich, and N. Lütkenhause, "Accessible nonlinear entanglement witnesses", Phys. Rev. A **85**, 062327 (2012).

[91] P. Horodecki, "From limits of quantum operations to multicopy entanglement witnesses and state-spectrum estimation", Phys. Rev. A **68**, 052101 (2003).

[92] L. Aolita and F. Mintert, "Measuring multipartite concurrence with a single factorizable observable", Phys. Rev. Lett. **97**, 050501 (2006).

[93] A. Salles, F. de Melo, M. P. Almeida, M. Hor-Meyll, S. P. Walborn, P. H. Souto Ribeiro, and L. Davidovich, "Experimental investigation of the dynamics of entanglement: sudden death, complementarity, and continuous monitoring of the environment", Phys. Rev. A **78**, 022322 (2008).

[94] A. Miranowicz, K. Bartkiewicz, J. Pe řina, M. Koashi, N. Imoto, and F. Nori, "Optimal two-qubit tomography based on local and global measurements: maximal robustness against errors as described by condition numbers", Phys. Rev. A **90**, 062123 (2014).

[95] K. Bartkiewicz, A. Černoch, K. Lemr, and A. Miranowicz, "Priority choice experimental two-qubit tomography: measuring one by one all elements of density matrices", Scientific Reports **6**, `10.1038/srep19610` (2016).

[96] Z. Hou, H.-S. Zhong, Y. Tian, D. Dong, B. Qi, L. Li, Y. Wang, F. Nori, G.-Y. Xiang, C.-F. Li, and et al., "Full reconstruction of a 14-qubit state within four hours", New Journal of Physics **18**, 083036 (2016).

[97] K. Bartkiewicz, K. Lemr, A. Černoch, and A. Miranowicz, "Bell nonlocality and fully entangled fraction measured in an entanglement-swapping device without quantum state tomography", Phys. Rev. A **95**, 030102 (2017).

[98] K. Bartkiewicz and G. Chimczak, "Two methods for measuring bell nonlocality via local unitary invariants of two-qubit systems in hong-ou-mandel interferometers", Phys. Rev. A **97**, 012107 (2018).

[99] F. A. Bovino, G. Castagnoli, A. Ekert, P. Horodecki, C. M. Alves, and A. V. Sergienko, "Direct measurement of nonlinear properties of bipartite quantum states", Phys. Rev. Lett. **95**, 240407 (2005).

[100] S. P. Walborn, P. H. S. Ribeiro, L. Davidovich, F. Mintert, and A. Buchleitner, "Experimental determination of entanglement with a single measurement", Nature **440**, 1022–1024 (2006).

[101] P. Badzia g, C. Brukner, W. Laskowski, T. Paterek, and M. Żukowski, "Experimentally friendly geometrical criteria for entanglement", Phys. Rev. Lett. **100**, 140403 (2008).

[102] M. Huber, F. Mintert, A. Gabriel, and B. C. Hiesmayr, "Detection of high-dimensional genuine multipartite entanglement of mixed states", Phys. Rev. Lett. **104**, 210501 (2010).

[103] O. Gühne, M. Reimpell, and R. F. Werner, "Estimating entanglement measures in experiments", Phys. Rev. Lett. **98**, 110502 (2007).

[104] B. Jungnitsch, T. Moroder, and O. Gühne, "Taming multiparticle entanglement", Phys. Rev. Lett. **106**, 190502 (2011).

[105] H. S. Park, S.-S. B. Lee, H. Kim, S.-K. Choi, and H.-S. Sim, "Construction of an optimal witness for unknown two-qubit entanglement", Phys. Rev. Lett. **105**, 230404 (2010).

[106] W. Laskowski, D. Richart, C. Schwemmer, T. Paterek, and H. Weinfurter, "Experimental schmidt decomposition and state independent entanglement detection", Phys. Rev. Lett. **108**, 240501 (2012).

[107] K. Bartkiewicz, P. Horodecki, K. Lemr, A. Miranowicz, and K. Życzkowski, "Method for universal detection of two-photon polarization entanglement", Phys. Rev. A **91**, 032315 (2015).

[108] K. Bartkiewicz, J. Beran, K. Lemr, M. Norek, and A. Miranowicz, "Quantifying entanglement of a two-qubit system via measurable and invariant moments of its partially transposed density matrix", Phys. Rev. A **91**, 022323 (2015).

[109] K. Bartkiewicz, G. Chimczak, and K. Lemr, "Direct method for measuring and witnessing quantum entanglement of arbitrary two-qubit states through hong-ou-mandel interference", Phys. Rev. A **95**, 022331 (2017).

[110] J. T. Barreiro, T.-C. Wei, and P. G. Kwiat, "Beating the channel capacity limit for linear photonic superdense coding", Nature Physics **4**, 282–286 (2008).

[111] C. Perumangatt, A. A. Rahim, G. R. Salla, S. Prabhakar, G. K. Samanta, G. Paul, and R. P. Singh, "Three-particle hyper-entanglement: teleportation and quantum key distribution", Quantum Information Processing **14**, 3813–3826 (2015).

[112] J. Cai, Z. Pan, T.-J. Wang, S. Wang, and C. Wang, "High-capacity quantum secure direct communication using hyper-entanglement of photonic qubits", International Journal of Quantum Information **14**, 1650043 (2016).

[113] M. Barbieri, C. Cinelli, P. Mataloni, and F. De Martini, "Polarization-momentum hyperentangled states: realization and characterization", Phys. Rev. A **72**, 052110 (2005).

[114] M. Barbieri, F. De Martini, P. Mataloni, G. Vallone, and A. Cabello, "Enhancing the violation of the einstein-podolsky-rosen local realism by quantum hyperentanglement", Phys. Rev. Lett. **97**, 140407 (2006).

[115] R. F. Werner, "Quantum states with einstein-podolsky-rosen correlations admitting a hidden-variable model", Phys. Rev. A **40**, 4277–4281 (1989).

[116] K. Bartkiewicz, K. Lemr, A. Černoch, J. Soubusta, and A. Miranowicz, "Experimental eavesdropping based on optimal quantum cloning", Phys. Rev. Lett. **110**, 173601 (2013).

[117] K. Bartkiewicz, A. Černoch, G. Chimczak, K. Lemr, A. Miranowicz, and F. Nori, "Experimental quantum forgery of quantum optical money", npj Quantum Information **3**, `10.1038/s41534-017-0010-x` (2017).

[118] X.-D. Cai, D. Wu, Z.-E. Su, M.-C. Chen, X.-L. Wang, L. Li, N.-L. Liu, C.-Y. Lu, and J.-W. Pan, "Entanglement-based machine learning on a quantum computer", Phys. Rev. Lett. **114**, 110504 (2015).

[119] K. Bartkiewicz, A. Černoch, K. Lemr, and A. Miranowicz, "Priority choice experimental two-qubit tomography: measuring one by one all elements of density matrices", Scientific Reports **6**, `10.1038/srep19610` (2016).

[120] C. Zhang, B. Yadin, Z.-B. Hou, H. Cao, B.-H. Liu, Y.-F. Huang, R. Maity, V. Vedral, C.-F. Li, G.-C. Guo, and D. Girolami, "Detecting metrologically useful asymmetry and entanglement by a few local measurements", Phys. Rev. A **96**, 042327 (2017).

[121] R. Filip, "Overlap and entanglement-witness measurements", Phys. Rev. A **65**, 062320 (2002).

[122] K. Bartkiewicz, K. Lemr, and A. Miranowicz, "Direct method for measuring of purity, superfidelity, and subfidelity of photonic two-qubit mixed states", Phys. Rev. A **88**, 052104 (2013).

[123] A. K. Ekert, C. M. Alves, D. K. L. Oi, M. Horodecki, P. Horodecki, and L. C. Kwek, "Direct estimations of linear and nonlinear functionals of a quantum state", Phys. Rev. Lett. **88**, 217901 (2002).

[124] T. A. Bruni, "Measurimg polynomial functions of states", Quantum Info. Comput. **4**, 401–408 (2004).

[125] H. Jeong, C. Noh, S. Bae, D. G. Angelakis, and T. C. Ralph, "Detecting the degree of macroscopic quantumness using an overlap measurement", J. Opt. Soc. Am. B **31**, 3057–3066 (2014).

[126] R. Islam, R. Ma, P. M. Preiss, M. E. Tai, A. Lukin, M. Rispoli, and M. Greiner, "Measuring entanglement entropy in a quantum many-body system", Nature **528**, 77–83 (2015).

[127] M. Paris and J. Řeháček, *Quantum state estimation* (Springer, 2011).

[128] K. Bartkiewicz, A. Černoch, K. Lemr, J. Soubusta, and M. Stobi ńska, "Efficient amplification of photonic qubits by optimal quantum cloning", Phys. Rev. A **89**, 062322 (2014).

[129] S. Pirandola, "Limits and security of free-space quantum communications", Physical Review Research **3** (2021).

[130] Z.-D. Li, R. Zhang, X.-F. Yin, L.-Z. Liu, Y. Hu, Y.-Q. Fang, Y.-Y. Fei, X. Jiang, J. Zhang, L. Li, and et al., "Experimental quantum repeater without quantum memory", Nature Photonics **13**, 644–648 (2019).

[131] T. Jennewein, G. Weihs, J.-W. Pan, and A. Zeilinger, "Experimental nonlocality proof of quantum teleportation and entanglement swapping", Phys. Rev. Lett. **88**, 017903 (2001).

[132] Z. Zhao, T. Yang, Y.-A. Chen, A.-N. Zhang, and J.-W. Pan, "Experimental realization of entanglement concentration and a quantum repeater", Phys. Rev. Lett. **90**, 207901 (2003).

[133] Z.-S. Yuan, Y.-A. Chen, B. Zhao, S. Chen, J. Schmiedmayer, and J.-W. Pan, "Experimental demonstration of a bdcz quantum repeater node", Nature **454**, 1098–1101 (2008).

[134] R. Kaltenbaek, B. Blauensteiner, M. Żukowski, M. Aspelmeyer, and A. Zeilinger, "Experimental interference of independent photons", Phys. Rev. Lett. **96**, 240502 (2006).

[135] M. Tanida, R. Okamoto, and S. Takeuchi, "Highly indistinguishable heralded single-photon sources using parametric down conversion", Opt. Express **20**, 15275–15285 (2012).

[136] S. K. Özdemir, K. Bartkiewicz, Y.-x. Liu, and A. Miranowicz, "Teleportation of qubit states through dissipative channels: conditions for surpassing the no-cloning limit", Phys. Rev. A **76**, 042325 (2007).

[137] Š. Chovancová, *Kvantové pravítko zrychlí umělou inteligenci a zvýší bezpečnost komunikace*, (2020 [online]) `https://www.zurnal.upol.cz/nc/zprava/clanek/kvantove-pravitko-zrychli-umelou-inteligenci-a-zvysi-bezpecnost-komunikace/`.

[138] *Odborníkům z olomoucké přírodovědy a fyzikálního ústavu se podařilo sestrojit unikátní kvantové pravítko*, (2020 [online]) `https://olomoucka.drbna.cz/zpravy/spolecnost/16982-odbornikum-z-olomoucke-prirodovedy-a-fyzikalniho-ustavu-se-podarilo-sestrojit-unikatni-kvantove-pravitko.html`.

[139] *Kvantové pravítko zrychlí umělou inteligenci*, (2020 [online]) `https://sciencemag.cz/kvantove-pravitko-zrychli-umelou-inteligenci/`.

Appendix

Faculty
of Science

Confirmation of contribution

As the supervisor to Mgr. Vojtěch Trávníček and corresponding author of his publications [1,2] and co-author of his publication [3]

[1] V. Trávníček, K. Bartkiewicz, A. Černoch, K. Lemr, "Experimental measurement of nonlinear entanglement witness by hyper-entangling two-qubit states," Phys. Rev. A **98**, 032307 (2018),

[2] V. Trávníček, K. Bartkiewicz, A. Černoch, and K. Lemr, "Experimental Diagnostics of Entanglement Swapping by a Collective Entanglement Test," Phys. Rev. Appl. **14**, 064071 (2020),

[3] V. Trávníček, K. Bartkiewicz, A. Černoch, K. Lemr, "Experimental Measurement of the Hilbert-Schmidt Distance between Two-Qubit States as a Means for Reducing the Complexity of Machine Learning," Phys. Rev. Lett. **123**, 260501 (2019)

I hereby certify that Mgr. Vojtěch Trávníček significantly contributed to the scientific investigation presented in these publications. Typically, he constructed the experimental setup, programmed the controlling software, processed the data and dominantly contributed to writing of the manuscripts. The extracts of the publications directly quoted in his thesis are of his own writing.

Olomouc, 10th April 2021

doc. Mgr. Karel Lemr, Ph.D.
Joint Laboratory of Optics

Palacký University Olomouc | Faculty of Science
17. listopadu1192/12 | CZ 771 46 Olomouc | Czech Republic | T: +420 585 634 060
www.prf.upol.cz

Faculty
of Science

Confirmation of contribution

As the co-author of Mgr. Vojtěch Trávníček publications:

[1] V. Trávníček, K. Bartkiewicz, A. Černoch, K. Lemr, "Experimental measurement of nonlinear entanglement witness by hyper-entangling two-qubit states," Phys. Rev. A **98**, 032307 (2018),

[2] V. Trávníček, K. Bartkiewicz, A. Černoch, and K. Lemr, "Experimental Diagnostics of Entanglement Swapping by a Collective Entanglement Test," Phys. Rev. Appl. **14**, 064071 (2020),

[3] V. Trávníček, K. Bartkiewicz, A. Černoch, K. Lemr, "Experimental Measurement of the Hilbert-Schmidt Distance between Two-Qubit States as a Means for Reducing the Complexity of Machine Learning," Phys. Rev. Lett. **123**, 260501 (2019)

I hereby certify that Mgr. Vojtěch Trávníček significantly contributed to the scientific investigation presented in these publications. Typically, he constructed the experimental setup, programmed the controlling software, processed the data and dominantly contributed to writing of the manuscripts. The extracts of the publications directly quoted in his thesis are of his own writing.

Olomouc, 26th April 2021 .....

Mgr. Antonín Černoch, Ph.D.
Joint Laboratory of Optics

Palacký University Olomouc | Faculty of Science
17. listopadu1192/12 | CZ 771 46 Olomouc | Czech Republic | T: +420 585 634 060
www.prf.upol.cz

ADAM MICKIEWICZ UNIVERSITY IN POZNAŃ
Faculty of Physics,
Institute of Spintronics and Quantum Information

Poznań, 28.04.2021

Confirmation of contribution

As an co-author of

[1] V. Trávníček, K. Bartkiewicz, A. Černoch, K. Lemr, "Experimental measurement of nonlinear entanglement witness by hyper-entangling two-qubit states," Phys. Rev. A **98**, 032307 (2018),

[2] V. Trávníček, K. Bartkiewicz, A. Černoch, and K. Lemr, "Experimental Diagnostics of Entanglement Swapping by a Collective Entanglement Test," Phys. Rev. Appl. **14**, 064071 (2020),

[3] V. Trávníček, K. Bartkiewicz, A. Černoch, K. Lemr, "Experimental Measurement of the Hilbert-Schmidt Distance between Two-Qubit States as a Means for Reducing the Complexity of Machine Learning," Phys. Rev. Lett. **123**, 260501 (2019)

I declare that Mgr. Vojtěch Trávníček contributed significantly to the scientific research presented in the above-listed publications. His contributions included constructing the experimental setups, programming the controlling software, and processing the data. He also contributed the most to writing the manuscripts.

Karol Bartkiewicz

Prof. UAM dr hab. Karol Bartkiewicz

Wydział Fizyki UAM, ul. Uniwersytetu Poznańskiego 2
61-614 Poznań, Poland,
Karol.Bartkiewicz@amu.edu.pl